PARP Inhibitor Upregulates PD-L1 Expression and Provides a New Combination Therapy in Pancreatic Cancer

Yali Wang[1, #], Kun Zheng[1, #], Yongbiao Huang[1], Xiuqiong Chen[1], Yilu Zhou[2,3], Wan Qin[1], Jinfang Su[1], Rui Chen[1], Hong Qiu[1], Xianglin Yuan[1], Hua Xiong[1], Yihua Wang[2, 3*], Yanmei Zou[1, *]

[1]Department of Oncology, Tongji Hospital, Tongji Medical College, Huazhong University of Science and Technology, Wuhan 430030, Hubei, China

[2]Biological Sciences, Faculty of Environmental and Life Sciences, University of Southampton, Southampton SO17 1BJ, UK

[3]Institute for Life Sciences, University of Southampton, Southampton, SO17 1BJ, UK

[#] These authors contributed equally to this study

[*] Correspondence should be addressed to Yanmei Zou (whtjzym@tjh.tjmu.edu.cn) or Yihua Wang (yihua.wang@soton.ac.uk)

Abstract

Despite recent improvements in treatment modalities, pancreatic cancer remains a highly lethal tumor with mortality rate increasing every year. Poly (ADP-ribose) polymerase (PARP) inhibitors are now used in pancreatic cancer as a breakthrough in targeted therapy. This study focused on whether PARP inhibitors (PARPis) can affect programmed death ligand-1 (PD-L1) expression in pancreatic cancer and whether immune checkpoint inhibitors of PD-L1/ programmed death 1 (PD-1) can enhance the anti-tumor effects of PARPis. Here we found that PARPi, pamiparib, up-regulated PD-L1 expression on the surface of pancreatic cancer cells *in vitro* and *in vivo*. Mechanistically, pamiparib induced PD-L1 expression via JAK2/STAT3 pathway in pancreatic cancer. Importantly, pamiparib attenuated tumor growth; while co-administration of pamiparib with PD-L1 blockers significantly improved the therapeutic efficacy *in vivo* compared with monotherapy. Combination therapy resulted in an altered tumor immune microenvironment with a significant increase in windiness of $CD8^+$ T cells, suggesting a potential role of $CD8^+$ T cells in the combination therapy. Together, this study provides evidence for the clinical application of PARPis with anti-PD-L1/PD-1 drugs in the treatment of pancreatic cancer.

Keywords: Pancreatic cancer; PARP inhibitors; pamiparib; PD-L1; $CD8^+$ T cells

Introduction

Pancreatic cancer is an extremely lethal disease with a poor prognosis. It ranks fourth and sixth, respectively, in causing cancer-related deaths in the USA and China [1], with a 5-year survival rate of less than 10% [2]. Although surgery is the only treatment with curative potential, a few chemotherapeutic agents could improve the prognosis of the pancreatic cancer [3]. For example, in addition to traditional chemotherapeutic agents such as gemcitabine or 5-fluorouracil, recent studies have shown that maintenance therapy with poly (ADP-ribose) polymerase (PARP) inhibitors is beneficial for patients with germline *BRCA* mutations and metastatic pancreatic cancer, and maybe a harbinger of progress in providing targeted therapy [4, 5].

PARP is a ribozyme involved in base excision repair, which transfers poly (ADP-ribose) (PAR) or mono-ADP-ribose to itself and/or other target proteins to sense and repair DNA damage [6, 7]. Among the PARP protein family, PARP-1 has a primary role in the total activity and occupies a central position in the repair of DNA single-strand breaks (SSBs) [8, 9]. PARP inhibitors (PARPis), whose most extensive mechanism of action is the inhibition on DNA damage repairing, have become promising for several cancer types, among which the clinical application of PARPis in ovarian cancer is the most advanced [10]. Olaparib is the first PARPi approved by the Food and Drug Administration (FDA) for the treatment of advanced *BRCA*-dependent ovarian cancer [11]. Pamiparib (BGB-290) is a highly selective PARP-1/2 inhibitor recently developed by BeiGene (Beijing) Co., Ltd. [12]. Its clinical trials in Chinese patients with advanced high-grade ovarian cancer and triple-negative breast cancer are in progress [13]. In addition, PARPis have shown great potential in pancreatic cancer, and several clinical trials are underway to assess PARPis as monotherapy or combination therapy that would be clinically effective in the treatment of pancreatic cancer [14-17]. Nevertheless, acquired resistance for PARPis has partially limited their use in clinical settings [18, 19]. Breakthroughs in immune checkpoint blockade therapies represent an important turning point in cancer immunotherapy, deepening our understanding of tumor immune evasion [20]. Programmed death 1 (PD-1) protein is a co-inhibitory receptor on the surface of activated T cells [21]. One of its known ligands, programmed death ligand-1 (PD-L1), is selectively expressed on the surface of tumor cells and in the tumor microenvironment [22, 23]. When PD-1 binds to PD-L1, activated T cells

receive inhibitory signals and cease to produce anti-tumor immune responses [21], rendering PD-L1 a potentially promising target for cancer immunotherapy [24, 25]. However, immune checkpoint inhibitors are ineffective in pancreatic cancer, probably because PD-L1 expression is consistently low in various cell subsets of pancreatic cancer [26-28].

In this study, we investigated the effects of PARPi, pamiparib, on pancreatic cancer and further explored its impact on the immune microenvironment. Here we found that pamiparib up-regulated PD-L1 expression on the surface of pancreatic cancer cells *in vitro and in vivo*. Mechanistically, pamiparib induced PD-L1 expression via JAK2/STAT3 pathway in pancreatic cancer. Importantly, pamiparib attenuated tumor growth; while co-administration of pamiparib with PD-L1 blockers significantly improved the therapeutic effect *in vivo* compared with monotherapy. Combination therapy resulted in an altered tumor immune microenvironment with a significant increase in windiness of $CD8^+$ T cells, suggesting a potential role of $CD8^+$ T cells in combination therapy. Together, this study provides evidence for the clinical application of PARPis with anti-PD-L1/PD-1 drugs in the treatment of pancreatic cancer.

Results

Pamiparib affects apoptosis, cell cycle, and proliferation in pancreatic cancer cells.

To explore whether pamiparib could alter functionalities of pancreatic cancer cells, we treated SW1990 cells with pamiparib (100 μM). By flow cytometry assay, it was observed that the use of pamiparib significantly induced apoptosis of pancreatic cancer cells compared to the control group ($P < 0.05$; Figure 1A). Further detection of cell cycle distribution by flow cytometry revealed that SW1990 cells were significantly blocked in G2/M phase upon pamiparib treatment in a time-dependent manner (all P values less than 0.01; Figure 1B). This suggests that pamiparib can significantly induce apoptosis and block cell cycle progression of pancreatic cancer cells *in vitro*.

To check the *in vivo* effects of pamiparib, we inoculated SW1990 cells subcutaneously on the back of nude mice. Pamiparib was administered by gavage twice daily at a dose of 3 mg/kg for 2 weeks, followed by tumor tissues isolation and embedding. Immunohistochemistry (IHC) staining of Ki-67 in tumor sections demonstrated that pamiparib treatment significantly inhibited the proliferation of tumor cells *in vivo* ($P < 0.01$; Figure 1C).

Effects of pamiparib treatment on PD-L1 expression.

Acquired resistance for PARPis partially limits its use in the pancreatic cancer [18, 19]. Their impacts on the immune microenvironment were investigated. We constructed a C57 mouse allograft tumor model using mouse pancreatic cancer cell line Pan-02, which was then gavaged with parmiparib. Tumor samples were excised for RNA sequencing (RNA-seq). CIBERSORT analysis was performed to calculate the abundance and immune fraction of 22 immune cells. A trend towards a suppressive effect on the expression of $CD4^+$ T cells and $CD8^+$ T cells was observed (Figure 2A). Using ESTIMATE calculations in R language, we found pamiparib treatment significantly reduced the immune score ($P < 0.05$; Figure 2B).

The results above suggested that pamiparib treatment could potentially lead to increased immunosuppression. Given the important role of PD-L1 upregulation in immunosuppression, we next investigated if pamiparib treatment in pancreatic cancer affects PD-L1 expression.

In vitro, we treated 2 different pancreatic cancer cells, SW1990 and BxPC-3, with

pamiparib and PD-L1 expressions was examined by both immunoblotting and flow cytometry. After treatment of both cell lines with pamiparib (100 μM), the results showed that pamiparib significantly increased total PD-L1 protein levels in both cell lines in a time-dependent manner (Figure 3A). The results of flow cytometry showed that PD-L1 expression on the surface of pancreatic cancer cells increased with time of administration after treatment with pamiparib in both cell lines (all *P* values less than 0.05; Figure 3B). We also treated SW1990 and BxPC-3 cell lines with different concentrations of pamiparib for 24h and found that the treatment increased PD-L1 protein expression in pancreatic cancer cells in a dose-dependent manner (Figure 3C).

The effects of pamiparib treatment on PD-L1 expressions *in vivo* were further investigated. Tumors of nude mice with subcutaneously inoculated SW1990 cells were observed. Pamiparib was administered to mice by gavage twice daily at a dose of 3 mg/kg for 2 weeks. Tumors were isolated from control or pamiparib-treated mice and stained for PD-L1 by IHC. The expression of PD-L1 was significantly higher in xenograft tumors of mice treated with pamiparib compared with untreated mice ($P < 0.01$; Figure 3D). Together, our results demonstrated that pamiparib treatment induces upregulation of PD-L1 expression in pancreatic cancer both *in vitro* and *in vivo*.

Pamiparib treatment induces PD-L1 expression via JAK2/STAT3 pathway.

To verify whether pamiparib -induced PD-L1 upregulation is required through the *PARP1* itself, we knocked down *PARP1* in SW1990 cells with siRNA against *PARP1* and treated the cells according to: (i) control group; (ii) pamiparib group; (iii) si*PARP1* group; (iv) pamiparib + si*PARP1* group for the experiment. Results suggested that PD-L1 expression was independent of *PARP1* levels (Supplementary Figure 1A). In order to find how pamiparib treatment regulates PD-L1 expression, we analyzed data from TCGA. We searched for pancreatic cancer in c-Bioportal, and genes that were positively correlated with PD-L1 (correlation coefficient ≥ 0.4) were identified and imported into STRING to construct a protein–protein interaction (PPI) co-expression network (Supplementary Figure 1B). KEGG enrichment (Supplementary Table 1) was performed to obtain pathways associated with PD-L1 regulation. We found that the

enriched pathways included NF-κB signaling pathway (false discovery rate, FDR = 0.0186), JAK-STAT signaling pathway (FDR = 0.00094), PI3K-AKT signaling pathway (FDR = 0.00014) and MAPK signaling pathway (FDR = 0.0014).

To test the potential roles of these pathways in regulating PD-L1 expression upon pamiparib treatment, SW1990 cells were pre-treated with pamiparib for 12 h, followed by the treatment of specific inhibitors targeting these pathways, including JAK-STAT signaling pathway (AG490) (Figure 4A), NF-kB signaling pathway (HY-N0274) (Supplementary Figure 2A), PI3K-AKT signaling pathway (LY294002) (Supplementary Figure 2B) and MAPK signaling pathway (SCH772984) (Supplementary Figure 2C). Results suggested an important role of JAK-STAT signaling pathway in mediating pamiparib-induced upregulation of PD-L1 (Figure 4A). Similar observations were noticed with inhibitors targeting PI3K-AKT or MAPK signaling pathway, but to a less extend (Supplementary Figure 2B and C). To further investigate the role of JAK-STAT signaling pathway, a specific inhibitor (stattic) against STAT3 was used and this treatment completely abolished the up-regulation of PD-L1 induced by pamiparib (Figure 4B).

We next investigated if pamiparib treatment could alter the activity of JAK-STAT signaling pathway. In SW1990 cells, pamiparib treatment activated JAK-STAT signaling pathway in a time-dependent manner, demonstrated by an increased level of phosphorylation in both JAK2 (Figure 4C) and STAT3 (Figure 4D). In addition, we also further explored the activation of PI3K-AKT signaling pathway and MAPK signaling pathway over time, and we found that the changes in phosphorylation of these two signaling pathways (Supplementary Figure 2D and E) did not coincide with the changes in PD-L1. Similar results were obtained *in vivo* by IHC staining of phospho-STAT3 (p-STAT3) (Figure 4E), with an increase upon pamiparib treatment ($P < 0.05$; Figure 4F). Together, the results demonstrated that pamiparib treatment induces PD-L1 expression via JAK2/STAT3 pathway.

Co-administration of pamiparib with PD-L1 blocker significantly improves the therapeutic efficacy *in vivo*.

Given the above observations that pamiparib treatment induces PD-L1 expressions, we next

investigated whether blocking PD-L1 could enhance the anti-cancer effects of pamiparib in pancreatic cancer. A C57 mouse allograft tumor model using mouse pancreatic cancer cell line Pan-02 was utilized to assess their efficacy. When the tumor volume reached 100 mm^3, mice were randomly divided into 4 groups for treatment (i.e., pamiparib monotherapy group, PD-L1 blocker monotherapy group, pamiparib and PD-L1 blocker combination group, and DMSO as a control group). Both pamiparib and anti-PD-L1 monotherapy significantly inhibited tumor growth. Interestingly, the combination therapy group achieved a better therapeutic effect compared to the monotherapy group (Figure 5A and B). The difference in body weight change was not statistically significant in mice receiving the combination treatment compared with mice in other experimental groups (Figure 5C). IHC staining of tumor specimens from mice showed that the combination treatment group had significantly fewer Ki-67 positive tumor cells than other groups (Figure 5D). These results indicated that the combination of PD-L1 blocker with pamiparib significantly inhibited the proliferative ability of tumors *in vivo*, i.e., enhanced the anti-cancer effect of pamiparib

Combination therapy with pamiparib and PD-L1 blocker increases T-cell infiltrations.

To understand the observations above, unbiased RNA sequencing (RNA-seq) was performed to quantify the changes in gene expression induced by pamiparib and/or anti-PD-L1 treatment. There are 936 differentially expressed genes (DEGs) (defined as $P < 0.05$ and fold change ≥ 2) between the untreated controls and combination therapy groups (Figure 6A). Functional classification of DEGs was performed based on gene ontology (GO). The top 10 most significantly enriched cellular components (CC), molecular functions (MF), biological processes (BP) between control and PD-L1 blocker-alone groups, control and pamiparib-alone groups, and control and combination groups are presented in Figure 6B-D and Supplementary Tables 2-4. Interestingly, all 3 treatments significantly altered "immune-related" genes, suggesting that both monotherapy and combination therapy modulate genes related to the immune response. A significant number of DEGs in combination therapy were also enriched in the categories of "inflammatory response", "innate immune response", "neutrophil accumulation" and "response to IFN-β response" categories, suggesting that combination

194 therapy significantly altered the expression of genes related to inflammation and the immune
195 system.

196 We, therefore, used CIBERSORT analysis to calculate the abundance and immune score
197 of 22 immune cell types. Both heat and box plots visualize that all components of $CD8^+$ T cells
198 were significantly higher in the combination treatment group compared to either the single-
199 agent group or the control group (e.g., initial $CD8^+$ T cells, memory $CD8^+$ T cells, killer $CD8^+$
200 T cells) (Figure 6E and F, Supplementary Figure 3). And the ratio of antigen-presenting cells
201 and macrophages also had a significant upregulation.

202 To verify the above findings, flow cytometry was used to examine whether the
203 combination treatment altered the tumor immune microenvironment. Increased infiltration of
204 $CD45^+$ immune cells in the combination group was observed by flow cytometry assay (Figure
205 7A, $P < 0.05$) and a significant decrease in MDSCs (Myeloid-derived suppressor cells)
206 infiltration (Figure 7B, $P < 0.05$). Similarly, the density of $CD8^+$ T cells was increased in the
207 combination treatment group (Figure 7C, $P < 0.05$).

208 Thus, the combination treatment of pamiparib and PD-L1 blocker could significantly alter
209 the tumor immune microenvironment, resulting in a significant upregulation of the proportion
210 of $CD8^+$ T cells.

211

212

Discussion

The prognosis of pancreatic cancer remains poor and no significant improvement has been achieved in the last two decades. Innovative findings are urgently needed to improve the 5-year survival rate of pancreatic cancer patients. Many studies have shown that the unique biological behavior of pancreatic cancer is related to the tumor microenvironment [29-31]. The immunosuppressive microenvironment of pancreatic cancer is highly heterogeneous, posing a challenge for immunotherapy. Immunotherapies that have received FDA approval for use in other tumors to date have little to no efficacy against this tumor. The problem lies in its strikingly immunosuppressive and "immune privileged" tumor microenvironment, where few patients exhibit robust T-cell infiltration [32]. Thus, pancreatic cancer has been classically described as a "cold" tumor in mice and humans because it is characterized by a relative paucity of intratumoral $CD8^+$ T cells [33]. A shift in the immunosuppressive microenvironment of the tumor contributes to the response to tumor immunotherapy [34]. Future treatments for pancreatic cancer will likely be based on the development of new therapies based on the genomic and proteomic identification of cellular/immune processes and molecular pathways as therapeutic targets [35].

Together with other reports in breast cancer [36], ovarian cancer [37], and non-small cell lung cancer [38], our study shows that simultaneous inhibition of PARP and PD-L1 confers therapeutic benefits. However, although the cytotoxic effects of PARPis have been well studied, the role of PARPis regarding how they modulate cancer-related immunity in pancreatic cancer remains largely unknown. Previously, it was revealed that PARPis upregulated PD-L1 expression through different pathways in breast and ovarian cancer, making the combination of the two more effective [36, 39]. In this study, we demonstrate that pamiparib upregulates PD-L1 expression through the JAK2/STAT3 pathway, at least partially (Figure 8), and that PD-L1 blockers enhance the effects of pamiparib *in vitro* and *in vivo*. Interestingly, although it has been suggested that tumors with *BRCA* mutations are sensitive to PARPis [40-41], findings from our study indicate that PD-L1 induction is not dependent on *BRCA* status, since similar results were obtained from the human pancreatic cancer cell line SW1990 and mouse pancreatic cancer cell line Pan-02, which have a *BRCA1* mutation, as well as the human pancreatic cancer

cell line BxPc-3 does not have mutations in either *BRCA1* or *BRCA2* (https://cancer.sanger.ac.uk/cell_lines/).

We show that combination treatment of PAPRi and anti-PD-L1 induces tumor regression in immunocompetent mice. The combination increases the infiltration of $CD8^+$ cytotoxic T cells and decreases the infiltration of MDSCs. As a result, the relatively poor presence of $CD8^+$ T cells in the immune microenvironment of pancreatic cancer is improved. Practically, these combinations are well tolerated in patients with combinations of 3 different PARPi (Olaparib [42], niraparib [43] and BGB-290 [44]) and PD-L1 or PD-1 antibodies being tested in a variety of cancer types (NCT02657889, NCT02484404 and NCT02660034). In this study, there are some limitations, including using a subcutaneous tumor model and no PD-L2 expression investigated. It has been suggested that orthotopic tumor models are more clinically relevant than their subcutaneous counterparts, although the latter is also widely used to study the immune microenvironment of pancreatic cancer [45-46]. Additionally, we reported that PD-L1 blockers enhance the effects of pamiparib *in vitro* and *in vivo*. The potential effects on PD-L2 are interesting and merit further investigation. Despite these limitations, our findings suggest a realistic scenario of a prospective clinical trial in pancreatic cancer patients with the combination therapy of PARPis and anti-PD-L1/PD-1.

Materials and methods

Mice, cell lines and reagents

All procedures were approved by the Institutional Animal Care and Use Committee of Tongji Medical College, Huazhong University of Science and Technology (approval number: TJH-201908003). Female C57BL/6 mice and BALB/c nude mice (6 weeks old) were obtained from the Jiangsu Jicui Pharmachem Experimental Animal Center. And the mice were housed in 5 animals per cage under standard laboratory conditions and fed with sterilized food and water. Mouse Pan02 and human-derived SW1990 and BxPC-3 pancreatic cancer cell lines were obtained from the Oncology Laboratory of Wuhan Tongji Hospital. Primary T cells were obtained from Wuhan Bio-Raid Biotechnology Co. Cancer cells were cultured in Dulbecco's modified Eagle's medium (DMEM) (HyClone, Logan, UT) supplemented with 10% fetal bovine serum (FBS) (Gibco, 10270-106, GER). Primary T cells were cultured by Metanni's Tex medium while activated with 100ng/mL CD3 antibody, 100ng/mL CD28 antibody and 10ng/mL IL2 (#317303; #302913; #589102, BioLegend). All cells were cultured in a humidified incubator at 37°C and 5% CO2. Pamiparib is one of PARPis, which was presented by BeiGene. No mycoplasma contamination was detected in the cell lines used. Anti-PD-L1 antibody (clone 10 F.9G2, Cat#BE0101) was purchased from BioXcell (West Lebanon, NH, USA).

Western blotting

The primary antibodies are PD-L1 (CST #13684, Cell Signaling Technology), PD-L1 (17952-1-AP, Santa Cruz), STAT3 (CST #9139, Cell Signaling Technology), phosphorylated STAT3 (CST #9145, Cell Signaling Technology), JAK2 (17670-1-AP, Proteintech), phosphorylated JAK2 (CST #4406, Cell Signaling Technology), AKT (10176-2-AP, Proteintech), phosphorylated AKT (66444-1-Ig, Proteintech), ERK (CST #4696, Cell Signaling Technology), phosphorylated ERK (CST #3510, Cell Signaling Technology), PARP-1 (sc-8007, Santa Cruz), and GAPDH (60004-1-Ig, Proteintech). Goat anti-rabbit antibody and mouse anti-rabbit antibody conjugated to HRP were purchased from Biosharp. all antibodies and reagents were stored and used according to the manufacturer's instructions. Briefly, tissues were homogenized,

mixed with 5X loading buffer and boiled until denaturation. Proteins were separated by sodium dodecyl sulfate-polyacrylamide gel electrophoresis and transferred to polyvinylidene difluoride membranes. Membranes are sealed with 5% skim milk and incubated overnight at 4°C with the primary antibody. The membranes were then washed, incubated with secondary antibodies for 1 hour at room temperature, and visualized with SuperSignal West Pico plus chemiluminescent substrate (Thermo Fisher Scientific, Waltham, MA).

Nude mice experiment

A dose of the drug was weighed and dissolved in a mixture of 10% DMSO, 5% Tween-80, 85% saline to form a solution of 12 mg/ml, which could be used for subsequent animal experiments in which mice were fed. SW1990 cell line was resuscitated, the cell status was adjusted to logarithmic cell growth, it was digested, centrifuged and the cell number was adjusted to 2x10^7/ml using serum-free medium. week-old male BALB/c nude mice were taken and 100ul of SW1990 cell suspension was injected into the right lower back of each nude mouse (i.e., the number of injections was 2 × 10^6). Tumor formation was observed, and when the tumor volume of mice was greater than 100 mm^3 (Tumor volume = (length × width × width)/2), the tumor size was sorted in order from largest to smallest, and the mice were sequentially divided into the experimental and control groups of pamiparib group. Mice in the experimental group were given oral pamiparib (3 mg/kg) twice daily, while mice in the control group were not given any special treatment. After 3 weeks of administration, the mice were executed and the tumor tissues were removed. The tissues were labeled and fixed in 4% paraformaldehyde. Paraffin-embedded tissues were used for subsequent experiments.

Drug treatments in mice

The cells were centrifuged after digestion and resuspended in the appropriate serum-free medium, and the density was adjusted to 2 × 10^7/ml after measuring the cell density with an automatic counting plate. All mice were housed in an SPF class mouse rearing room and fed with water freely. All animals were housed and operated following the relevant regulatory and ethical requirements for experimental animals. When the tumor volume was larger than 100

mm^3, the mice were sorted according to the size of the tumor from the largest to the smallest, and after ear tagging, each mouse was randomly assigned to each experimental group and pair according to the principle of random assignment, and they were randomly divided into 4 groups (6 mice in each group). The mice were divided into four groups: (i) control group; (ii) PD-L1 inhibitor group; (iii) pamiparib monotherapy group; and (iv) PD-L1 inhibitor and pamiparib combination group. The mice in the pamiparib group were fed twice daily with 3 mg/kg each time. pamiparib mice in the PD-L1 group were injected intraperitoneally with murine PD-L1 antibody at 10 mg/kg each time every 3 d. Both pamiparib and PD-L1 were administered in the same way as in the first two groups. Tumor volume and body weight were measured by digital calipers and electronic scales every 3 days. After 4 injections of anti-mouse PD-L1 antibody, the mice were executed, the tumor tissues were removed and photographed. A straightedge needs to be placed at the time of photographing, which can be used to calculate the tumor volume later. The tissues were processed differently, and one part was collected for flow cytometry detection. One part was fixed in 4% paraformaldehyde and embedded in paraffin. Paraffin-embedded tissue sections are stained for H&E and IHC. A portion was frozen in liquid nitrogen for RNA-seq.

Transfections

After digesting the SW1990 cell line in a logarithmic growth phase, adjust the cell number to 1×10^5/ml using the medium in the absence of resistance, inoculate 1 ml of cell suspension in each well of the six-well plate, and wait for the cell fusion to be 30-50% for subsequent transfection experiments. (Note: When spreading the plate, the cells should be digested and mixed completely to avoid cell pile-up growth. Dilute si*PARP1* (final concentration of transfected cells is 50nM) with 50 ul Opti-MEM and mix by gently blowing 3~5 times. Mix the transfection reagent and si*PARP1* dilution by gently inverting, dilute 1.0 ul LipofectamineTM 2000 with 50 ul Opti-MEM, gently blow 3~5 times to mix, and let stand at room temperature for 5 min. The transfection complex was added to 6-well cell plates, 100μL/well, and the plates were gently shaken before and after to mix well. The plates were incubated at 37°C, 5% CO2, in an incubator for 18~48 h. After transfection for 4~6 h, the media

could be changed to fresh ones.

Flow cytometry

Tumor sections were weighed, cut into small pieces, and digested with Mouse Tumor Dissociation Kit (Cat# 130-096-730, Miltenyi Biotec) enzyme cocktail solution at 37°C for 30 minutes. Add PBS containing 1% fetal bovine serum to stop the reaction. Cells were pelleted at 1200 rpm for 5 min at 4°C, resuspended in phosphate-buffered saline, and mashed through a 70 μm cell filter. To detect the lymphocyte component of the infiltrating tumor microenvironment, cells were stained with the antibodies listed in Supplementary Table 5 according to the protocol for flow cytometry. Data were collected with a CytoFLEX S (Beckman Coulter) or BD LSRII cytometer and analyzed with FlowJo software (version 7.6; Tree Star, Ashland, OR, USA). Cell populations were quantified by gating from single-stained positive controls and fluorescent minus one (FMO) controls.

RNA sequencing (RNA-seq)

mRNA sequencing was performed by Illumina HiSe, and total RNA from each sample was extracted using TRIzol Reagent (Invitrogen)/RNeasy Mini Kit (Qiagen)/other kits for the preparation of the following libraries. The PCR products were washed with beads, validated with Qsep100 (Bioptic, Taiwan, China), and quantified with a Qubit 3.0 fluorometer (Invitrogen, Carlsbad, CA, USA). Libraries of different indices were multiplexed and loaded on an Illumina HiSeq instrument (Illumina, San Diego, CA, USA) according to the manufacturer's instructions. Sequencing was performed using a 2x150bp paired-end (PE) configuration; image analysis and base calling were performed on the HiSeq instrument by HiSeq Control Software (HCS) + OLB + GAPipeline-1.6 (Illumina). Sequences were processed and analyzed by GENEWIZ. The CIBERSORT analysis used for the subsequent calculation of the abundance and immune score of the 22 immune cells was drawn by ggplot. RNA-seq data have been deposited in NCBI database (accession code PRJNA724048).

Immunohistochemistry

After antigen repair place in 5% BSA and incubated for 20 min for closure. At 4°C with the corresponding primary antibodies (PD-L1 (1:200, CST #13684, Cell Signaling Technology), phospho-STAT3 (1:200, CST #9145, Cell Signaling Technology), Ki-67 (1:200, ab16667, Abcam)) were incubated overnight. After overnight incubation, sections were rinsed 3 times with PBS solution for 5 min each. sections were placed in antibody solution, incubated with secondary antibody at 37 °C for 30 min, and then rinsed 3 times with PBS solution for 5 min each. Stained, and blocking, IHC results were scored immunohistochemically by two independent observers.

Bioinformatic analysis

We searched for Pancreatic cancer in c-Bioportal, then searched for genes positively correlated with CD274 co-expression, then imported the genes with cor ≥ 0.4 into STRING, constructed the co-expression network and then analyzed them. We obtained pathways associated with PD-L1 regulation from KEGG analysis.

Statistical analysis

Statistical analyses were conducted using SPSS version 26.0 software (SPSS Inc., Chicago, USA) and GraphPad Prism software (GraphPad version 8.0). The IHC results were analyzed by Pearson χ^2 test. Data were displayed as mean ± SEM. Differences between variables were analyzed by one-way ANOVA or two-tailed Student's t-test for *P*-values. Differences were considered statistically significant at $P < 0.05$ (*). Each experiment was repeated at least 3 times.

Acknowledgements

This project was supported by the National Natural Science Foundation of China [81772827].

Author Contributions

YZ and YW conceived, designed, and managed the study; YW, KZ, YH, XC, YZ, WQ, JS, and RC performed the experiments; YW, KZ, HQ, XY, HX, YW and YZ drafted the manuscript; All authors approved the final manuscript.

Conflict of Interest

The authors declare that the research was conducted in the absence of any commercial or financial relationships that could be construed as a potential conflict of interest.

Figure Legends

Figure 1. Pamiparib affects apoptosis, cell cycle, and proliferation in pancreatic cancer cells. (A) Flow cytometry detection of cell apoptosis showing pamiparib treatment causes a significant increase of apoptosis in SW1990 cells. (B) Flow cytometry detection of cell cycle showing pamiparib blocks SW1990 cells in G2/M phase. (C) IHC staining of Ki-67 showing pamiparib inhibits the proliferation of SW1990 cells in the in vivo environment. Data are mean ± SD; n = 3 samples per group. Scale bar, 100 μm. The IHC results were analyzed by Pearson $\chi 2$ test. *P < 0.05, **P < 0.01, ***P < 0.001, ns differences are not statistically significant.

Figure 2. Bioinformatic analysis of RNA-seq dataset from a Pan-02 allograft tumor model treated with parmiparib. (A) Spectrograms of 22 immune cell expressions in 2 different groups. Control, control group; pamiparib, pamiparib monotherapy group. (B) Histogram of immune scores between the 2 groups. Control, control group; pamiparib, pamiparib monotherapy group. Data are mean ± SD; n = 5 samples per group. Data analysis was performed by unpaired t-test. *P < 0.05, **P < 0.01, ***P < 0.001, ns differences are not statistically significant.

Figure 3. Effects of pamiparib treatment on PD-L1 expression. (A) SW1990 and BxPC-3 cells were treated with pamiparib, proteins were extracted at selected time points (0h, 6h, 12h, 24h), and PD-L1 protein expression was found to be up-regulated by immunoblotting. (B) Flow cytometry detection of PD-L1 expression on the surface of SW1990 and BxPC-3 cells after pamiparib treatment for different times. The flow cytometry results were analyzed by unpaired t-test. (C) PD-L1 protein expression was detected by immunoblotting after treatment of SW1990 and BxPC-3 cells with different concentrations of pamiparib for 24h (0, 5, 10, 15μM). (D) PD-L1 expression showed significant differences under IHC staining in control and nude mouse xenograft tumors treated with pamiparib. Control, control group; pamiparib, pamiparib monotherapy group. Data are mean ± SD; n = 3 samples per group. Scale bar, 100 μm. The IHC results were analyzed by Pearson $\chi 2$ test. *P < 0.05, **P < 0.01, ***P < 0.001, ns differences were not statistically significant.

Figure 4. Pamiparib treatment induces PD-L1 expression via JAK2/STAT3 pathway. (A) Cells were pretreated with pamiparib (100 μM, 12h) and PD-L1 expression was assessed by immunoblotting after treatment with the concentrations (20 μM) of AG490 for 24h. (B) Cells were pretreated with pamiparib (100 μM, 12h) and PD-L1 expression was assessed by protein blotting after treatment with stattic (20 μM) for 24h. (C) Protein expression of phospho-JAK2 (p-JAK2), JAK2, and PD-L1 in SW1990 cells after being treated with pamiparib (100 μM) for the indicated times. (D) Protein expression of phospho-STAT3(p-STAT3), STAT3 and PD-L1 in SW1990 cells after being treated with pamiparib (100 μM) for the indicated times. GAPDH was used as a loading control. (E) Expression of p-STAT3 was significantly upregulated in IHC staining of nude mice. Data are mean ± SD; n = 3 samples per group. Scale bar, 100 μm. The IHC results were analyzed by Pearson $\chi 2$ test. *P < 0.05, **P < 0.01, ***P < 0.001, ns differences were not statistically significant.

Figure 5. Co-administration of pamiparib with PD-L1 blocker significantly improves the therapeutic effect *in vivo*. (A) Tumor volume curves of C57 mice carrying Pan-02 allograft tumors in different treatment groups (n = 6) and tumor pictures at the end of treatment. (B) Tumor weight histograms of Pan-02 allograft mice in different treatment groups (n = 6). (C) Bodyweight curves of mice in four different treatment groups at the indicated time points after receiving treatment. Data analysis was performed by unpaired t-test. (D) Representative images of H&E and Ki-67 IHC staining of Pan-02 allograft tumors in mice from different treatment groups (n = 5). Scale bar, 100 μm. (E) IHC staining and scores showing consistent trends in PD-L1 and p-STAT3 changes were observed between the four groups of C57 (n = 5). Scale bar, 100 μm. *P < 0.05, **P < 0.01, ***P < 0.001, ns differences were not statistically significant.

Figure 6. Bioinformatic analysis suggests that combination therapy with pamiparib and PD-L1 blocker alters the immune microenvironment. (A) Volcano plot for differential genes between control and combination treatment groups. (B) Bar plot showing the top 10 enriched CC, MF and BP terms between the PD-L1 inhibitor group (PD-L1) and the control group. (C) Bar plot showing the top 10 enriched CC, MF and BP terms between pamiparib monotherapy group

(BGB290) and the control group. (D) Bar plot showing the top 10 enriched CC, MF and BP terms between PD-L1 inhibitor and pamiparib combination group (Combine) and the control group. Green indicates CC term, red indicates MF term and blue indicates BP term. The numbers indicate the numbers of enriched genes in each term. (E) Heat map of 22 immune cells expression in four different groups. (F) Boxplot of 22 immune cell infiltrations in four different groups. Data analysis was performed by unpaired t-test. *$P < 0.05$, **$P < 0.01$, ***$P < 0.001$, ns differences are not statistically significant.

Figure 7. Flow cytometry analysis confirms that combination therapy with pamiparib and PD-L1 blocker alters the immune microenvironment. (A-C) Flow cytometry analysis to calculate the ratio values of $CD45^+$ cells (A), MDSC cells (B) and $CD8^+$ T cells (C) per 1.0 g of tumor tissue. *$P < 0.05$.

Figure 8. Diagram summarizing that pamiparib treatment induces PD-L1 expression mainly via JAK2/STAT3 in pancreatic cancer (details provided in the Discussion section).

References

[1] Cao W, Chen HD, Yu YW, Li N, Chen WQ. Changing profiles of cancer burden worldwide and in China: a secondary analysis of the global cancer statistics 2020. Chin Med J (Engl). 2021; 134: 783-791.

[2] Siegel RL, Miller KD, Jemal A. Cancer statistics, 2020. CA: a cancer journal for clinicians. 2020; 70: 7-30.

[3] Doi T, Ishikawa T, Okayama T, Oka K, Mizushima K, Yasuda T*, et al.* The JAK/STAT pathway is involved in the upregulation of PD-L1 expression in pancreatic cancer cell lines. Oncol Rep. 2017; 37: 1545-1554.

[4] Golan T, Hammel P, Reni M, Van Cutsem E, Macarulla T, Hall MJ*, et al.* Maintenance Olaparib for Germline BRCA-Mutated Metastatic Pancreatic Cancer. N Engl J Med. 2019; 381: 317-327.

[5] Liu X, Yang J, Zhang Y, Fang Y, Wang F, Wang J*, et al.* A systematic study on drug-response associated genes using baseline gene expressions of the Cancer Cell Line Encyclopedia. Sci Rep. 2016; 6: 22811.

[6] Zhu H, Wei M, Xu J, Hua J, Liang C, Meng Q*, et al.* PARP inhibitors in pancreatic cancer: molecular mechanisms and clinical applications. Mol Cancer. 2020; 19: 49.

[7] Liu C, Wei D, Xiang J, Ren F, Huang L, Lang J*, et al.* An Improved Anticancer Drug-Response Prediction Based on an Ensemble Method Integrating Matrix Completion and Ridge Regression. Mol Ther Nucleic Acids. 2020; 21: 676-686.

[8] Eustermann S, Wu WF, Langelier MF, Yang JC, Easton LE, Riccio AA*, et al.* Structural Basis of Detection and Signaling of DNA Single-Strand Breaks by Human PARP-1. Mol Cell. 2015; 60: 742-754.

[9] McLornan DP, List A, Mufti GJ. Applying synthetic lethality for the selective targeting of cancer. N Engl J Med. 2014; 371: 1725-1735.

[10] Farmer H, McCabe N, Lord CJ, Tutt AN, Johnson DA, Richardson TB*, et al.* Targeting the DNA repair defect in BRCA mutant cells as a therapeutic strategy. Nature. 2005; 434: 917-921.

[11] Sonnenblick A, de Azambuja E, Azim HA, Jr., Piccart M. An update on PARP inhibitors--moving to the adjuvant setting. Nat Rev Clin Oncol. 2015; 12: 27-41.

[12] Wang H, Ren B, Liu Y, Jiang B, Guo Y, Wei M*, et al.* Discovery of Pamiparib (BGB-290), a Potent and Selective Poly (ADP-ribose) Polymerase (PARP) Inhibitor in Clinical Development. J Med Chem. 2020; 63: 15541-15563.

[13] Xu B, Yin Y, Dong M, Song Y, Li W, Huang X*, et al.* Pamiparib dose escalation in Chinese patients with non-mucinous high-grade ovarian cancer or advanced triple-negative breast cancer. Cancer Med. 2021; 10: 109-118.

[14] Lowery MA, Kelsen DP, Capanu M, Smith SC, Lee JW, Stadler ZK*, et al.* Phase II trial of veliparib in patients with previously treated BRCA-mutated pancreas ductal adenocarcinoma. Eur J Cancer. 2018; 89: 19-26.

[15] Tuli R, Shiao SL, Nissen N, Tighiouart M, Kim S, Osipov A*, et al.* A phase 1 study of veliparib, a PARP-1/2 inhibitor, with gemcitabine and radiotherapy in locally advanced pancreatic cancer. EBioMedicine. 2019; 40: 375-381.

[16] Bendell J, O'Reilly EM, Middleton MR, Chau I, Hochster H, Fielding A*, et al.* Phase I study

of olaparib plus gemcitabine in patients with advanced solid tumours and comparison with gemcitabine alone in patients with locally advanced/metastatic pancreatic cancer. Ann Oncol. 2015; 26: 804-811.

[17] Yang J, Peng S, Zhang B, Houten S, Schadt E, Zhu J, *et al.* Human geroprotector discovery by targeting the converging subnetworks of aging and age-related diseases. Geroscience. 2020; 42: 353-372.

[18] Konstantinopoulos PA, Ceccaldi R, Shapiro GI, D'Andrea AD. Homologous Recombination Deficiency: Exploiting the Fundamental Vulnerability of Ovarian Cancer. Cancer Discov. 2015; 5: 1137-1154.

[19] Lord CJ, Ashworth A. Mechanisms of resistance to therapies targeting BRCA-mutant cancers. Nat Med. 2013; 19: 1381-1388.

[20] Couzin-Frankel J. Breakthrough of the year 2013. Cancer immunotherapy. Science. 2013; 342: 1432-1433.

[21] Okazaki T, Honjo T. PD-1 and PD-1 ligands: from discovery to clinical application. Int Immunol. 2007; 19: 813-824.

[22] Dong H, Strome SE, Salomao DR, Tamura H, Hirano F, Flies DB, *et al.* Tumor-associated B7-H1 promotes T-cell apoptosis: a potential mechanism of immune evasion. Nat Med. 2002; 8: 793-800.

[23] Zou W, Chen L. Inhibitory B7-family molecules in the tumour microenvironment. Nat Rev Immunol. 2008; 8: 467-477.

[24] Brahmer JR, Tykodi SS, Chow LQ, Hwu WJ, Topalian SL, Hwu P, *et al.* Safety and activity of anti-PD-L1 antibody in patients with advanced cancer. N Engl J Med. 2012; 366: 2455-2465.

[25] Yang Y. Cancer immunotherapy: harnessing the immune system to battle cancer. J Clin Invest. 2015; 125: 3335-3337.

[26] Balli D, Rech AJ, Stanger BZ, Vonderheide RH. Immune Cytolytic Activity Stratifies Molecular Subsets of Human Pancreatic Cancer. Clinical cancer research : an official journal of the American Association for Cancer Research. 2017; 23: 3129-3138.

[27] Xu J, Cai L, Liao B, Zhu W, Yang J. CMF-Impute: an accurate imputation tool for single-cell RNA-seq data. Bioinformatics. 2020; 36: 3139-3147.

[28] Zhuang J, Cui L, Qu T, Ren C, Yang J. A streamlined scRNA-Seq data analysis framework based on improved sparse subspace clustering. IEEE Access. 2021; PP: 1-1.

[29] Sasaki K, Takano S, Tomizawa S, Miyahara Y, Furukawa K, Takayashiki T, *et al.* C4b-binding protein α-chain enhances antitumor immunity by facilitating the accumulation of tumor-infiltrating lymphocytes in the tumor microenvironment in pancreatic cancer. J Exp Clin Cancer Res. 2021; 40: 212.

[30] Sun K, Zhang XD, Liu XY, Lu P. YAP1 is a Prognostic Biomarker and Correlated with Immune Cell Infiltration in Pancreatic Cancer. Front Mol Biosci. 2021; 8: 625731.

[31] Zhang C, Ding J, Xu X, Liu Y, Huang W, Da L, *et al.* Tumor Microenvironment Characteristics of Pancreatic Cancer to Determine Prognosis and Immune-Related Gene Signatures. Front Mol Biosci. 2021; 8: 645024.

[32] Wu J, Cai J. Dilemma and Challenge of Immunotherapy for Pancreatic Cancer. Digestive diseases and sciences. 2021; 66: 359-368.

[33] Hussain I, Rashid MU, Sarvepalli D, Rahman AU, Ullah W, Badar H, *et al.* Newer Trends in

Pancreatic Cancer Treatment: Genetic Alterations and the Role of Immune Therapeutic and Targeted Therapies. Critical reviews in oncogenesis. 2019; 24: 157-177.

[34] Lord CJ, Ashworth A. PARP inhibitors: Synthetic lethality in the clinic. Science. 2017; 355: 1152-1158.

[35] Han Y, Liu D, Li L. PD-1/PD-L1 pathway: current researches in cancer. American journal of cancer research. 2020; 10: 727-742.

[36] Jiao S, Xia W, Yamaguchi H, Wei Y, Chen MK, Hsu JM, *et al.* PARP Inhibitor Upregulates PD-L1 Expression and Enhances Cancer-Associated Immunosuppression. Clin Cancer Res. 2017; 23: 3711-3720.

[37] Färkkilä A, Gulhan DC, Casado J, Jacobson CA, Nguyen H, Kochupurakkal B, *et al.* Immunogenomic profiling determines responses to combined PARP and PD-1 inhibition in ovarian cancer. Nature communications. 2020; 11: 1459.

[38] Sen T, Rodriguez BL, Chen L, Corte CMD, Morikawa N, Fujimoto J, *et al.* Targeting DNA Damage Response Promotes Antitumor Immunity through STING-Mediated T-cell Activation in Small Cell Lung Cancer. Cancer Discov. 2019; 9: 646-661.

[39] Xue C, Xu Y, Ye W, Xie Q, Gao H, Xu B, *et al.* Expression of PD-L1 in ovarian cancer and its synergistic antitumor effect with PARP inhibitor. Gynecologic oncology. 2020; 157: 222-233.

[40] Moschetta M, George A, Kaye SB, Banerjee S. BRCA somatic mutations and epigenetic BRCA modifications in serous ovarian cancer. Ann Oncol. 2016; 27: 1449-1455.

[41] Robson M, Im SA, Senkus E, Xu B, Domchek SM, Masuda N, *et al.* Olaparib for Metastatic Breast Cancer in Patients with a Germline BRCA Mutation. N Engl J Med. 2017; 377: 523-533.

[42] Domchek SM, Postel-Vinay S, Im SA, Park YH, Delord JP, Italiano A, *et al.* Olaparib and durvalumab in patients with germline BRCA-mutated metastatic breast cancer (MEDIOLA): an open-label, multicentre, phase 1/2, basket study. Lancet Oncol. 2020; 21: 1155-1164.

[43] Konstantinopoulos PA, Waggoner S, Vidal GA, Mita M, Moroney JW, Holloway R, *et al.* Single-Arm Phases 1 and 2 Trial of Niraparib in Combination With Pembrolizumab in Patients With Recurrent Platinum-Resistant Ovarian Carcinoma. JAMA oncology. 2019; 5: 1141-1149.

[44] Friedlander M, Meniawy T, Markman B, Mileshkin L, Harnett P, Millward M, *et al.* Pamiparib in combination with tislelizumab in patients with advanced solid tumours: results from the dose-escalation stage of a multicentre, open-label, phase 1a/b trial. The Lancet Oncology. 2019; 20: 1306-1315.

[45] Mace TA, Shakya R, Pitarresi JR, Swanson B, McQuinn CW, Loftus S, *et al.* IL-6 and PD-L1 antibody blockade combination therapy reduces tumour progression in murine models of pancreatic cancer. Gut. 2018; 67: 320-332.

[46] Azad A, Yin Lim S, D'Costa Z, Jones K, Diana A, Sansom OJ, *et al.* PD-L1 blockade enhances response of pancreatic ductal adenocarcinoma to radiotherapy. EMBO Mol Med. 2017; 9: 167-180.

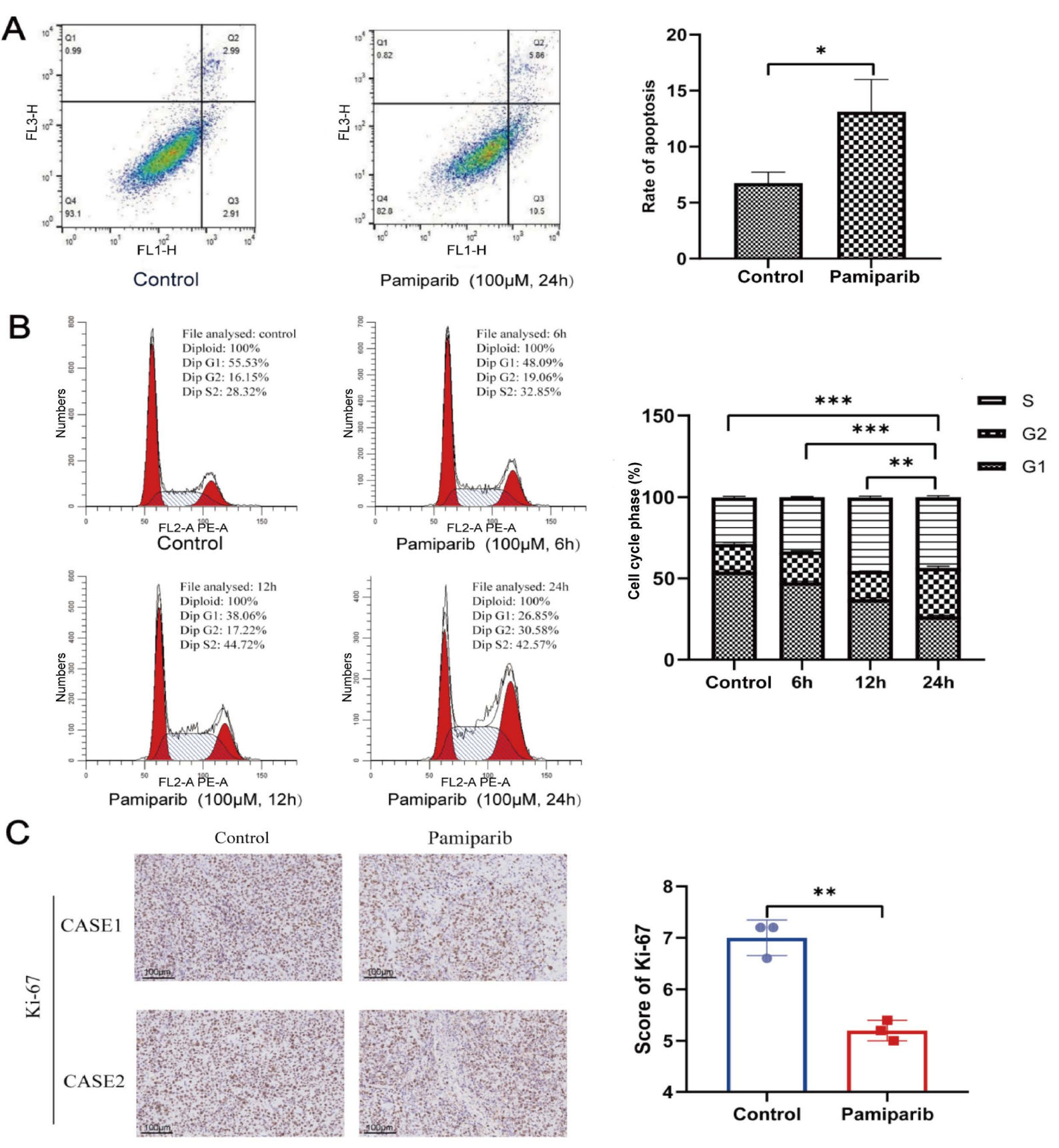
A
Q1
0.99
Q2
2.99
Q4
93.1
Q3
2.91
FL3-H
FL1-H
Control
Q1
0.82
Q2
5.86
Q4
82.8
Q3
10.5
FL3-H
FL1-H
Pamiparib (100μM, 24h)
Rate of apoptosis
20
15
10
5
0
*
Control
Pamiparib
B
File analysed: control
Diploid: 100%
Dip G1: 55.53%
Dip G2: 16.15%
Dip S2: 28.32%
Numbers
FL2-A PE-A
Control
File analysed: 6h
Diploid: 100%
Dip G1: 48.09%
Dip G2: 19.06%
Dip S2: 32.85%
Numbers
FL2-A PE-A
Pamiparib (100μM, 6h)
File analysed: 12h
Diploid: 100%
Dip G1: 38.06%
Dip G2: 17.22%
Dip S2: 44.72%
Numbers
FL2-A PE-A
Pamiparib (100μM, 12h)
File analysed: 24h
Diploid: 100%
Dip G1: 26.85%
Dip G2: 30.58%
Dip S2: 42.57%
Numbers
FL2-A PE-A
Pamiparib (100μM, 24h)
Cell cycle phase (%)
150
100
50
0
***
***
**
S
G2
G1
Control
6h
12h
24h
C
Control
Pamiparib
Ki-67
CASE1
CASE2
100μm
Score of Ki-67
8
7
6
5
4
**
Control
Pamiparib

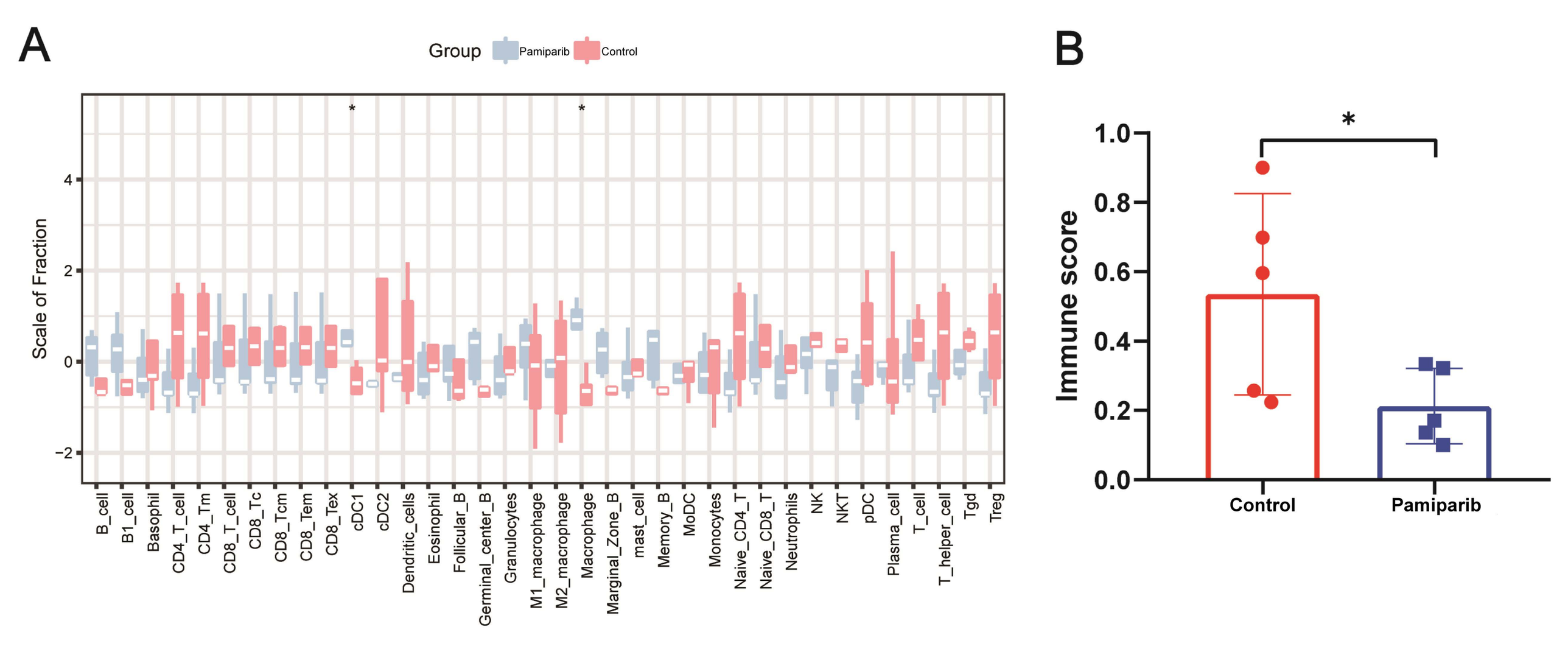
A
Group
Pamiparib
Control
Scale of Fraction
4
2
0
−2
*
*
B_cell
B1_cell
Basophil
CD4_T_cell
CD4_Tm
CD8_T_cell
CD8_Tc
CD8_Tcm
CD8_Tem
CD8_Tex
cDC1
cDC2
Dendritic_cells
Eosinophil
Follicular_B
Germinal_center_B
Granulocytes
M1_macrophage
M2_macrophage
Macrophage
Marginal_Zone_B
mast_cell
Memory_B
MoDC
Monocytes
Naive_CD4_T
Naive_CD8_T
Neutrophils
NK
NKT
pDC
Plasma_cell
T_cell
T_helper_cell
Tgd
Treg
B
Immune score
1.0
0.8
0.6
0.4
0.2
0.0
*
Control
Pamiparib

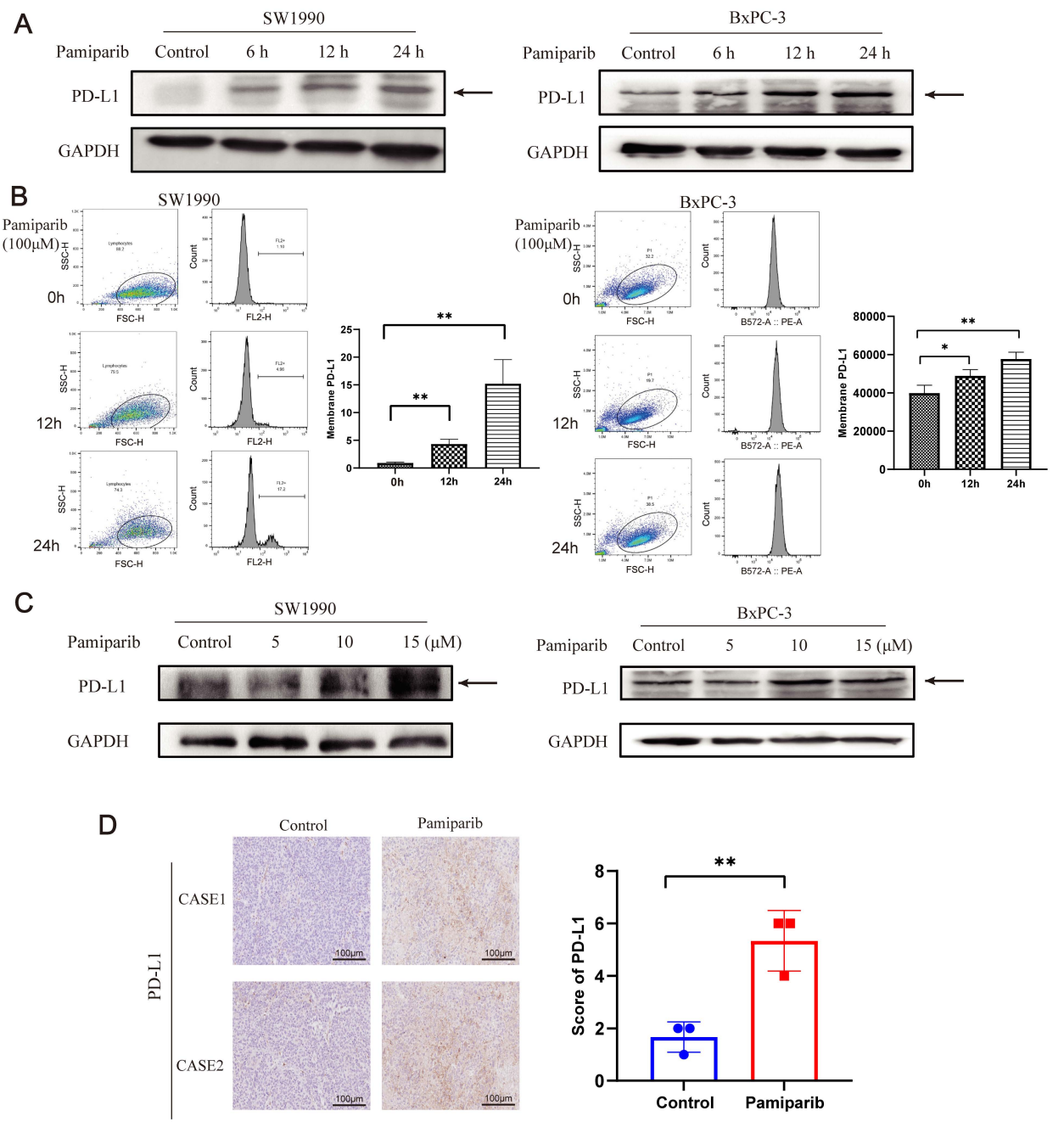
A
SW1990
Pamiparib
Control
6 h
12 h
24 h
PD-L1
GAPDH
BxPC-3
B
SW1990
BxPC-3
Pamiparib (100μM)
0h
12h
24h
SSC-H
FSC-H
Count
FL2-H
B572-A :: PE-A
Membrane PD-L1
**
*
C
SW1990
BxPC-3
Control
5
10
15 (μM)
D
Control
Pamiparib
CASE1
CASE2
100μm
Score of PD-L1

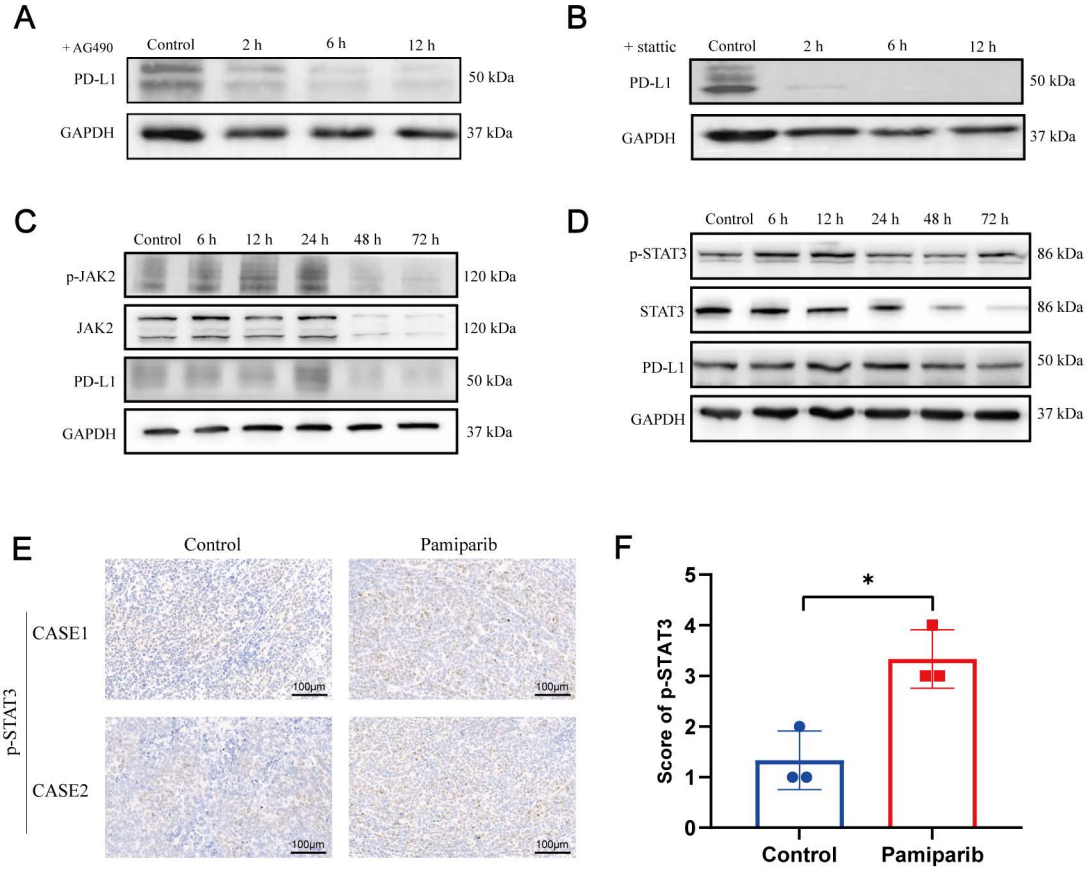
A
+ AG490
Control
2 h
6 h
12 h
PD-L1
50 kDa
GAPDH
37 kDa
B
+ stattic
Control
2 h
6 h
12 h
PD-L1
50 kDa
GAPDH
37 kDa
C
Control
6 h
12 h
24 h
48 h
72 h
p-JAK2
120 kDa
JAK2
120 kDa
PD-L1
50 kDa
GAPDH
37 kDa
D
Control
6 h
12 h
24 h
48 h
72 h
p-STAT3
86 kDa
STAT3
86 kDa
PD-L1
50 kDa
GAPDH
37 kDa
E
Control
Pamiparib
p-STAT3
CASE1
CASE2
100μm
F
Score of p-STAT3
*
Control
Pamiparib

A

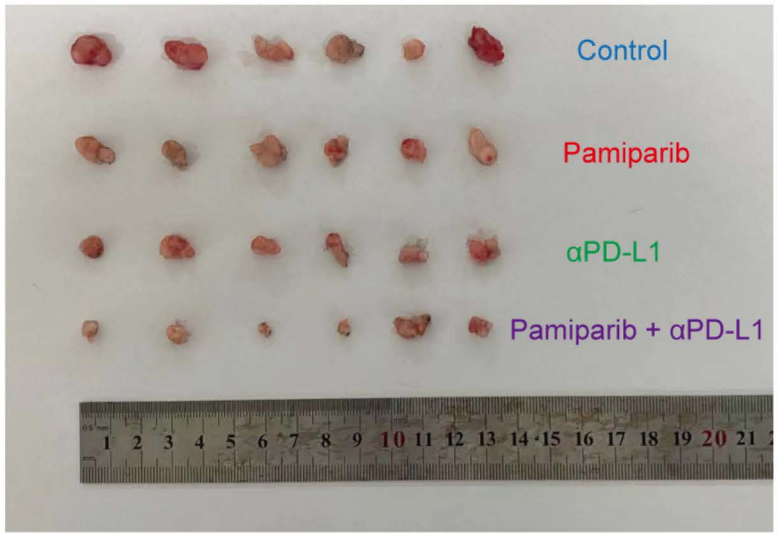
Control
Pamiparib
αPD-L1
Pamiparib + αPD-L1

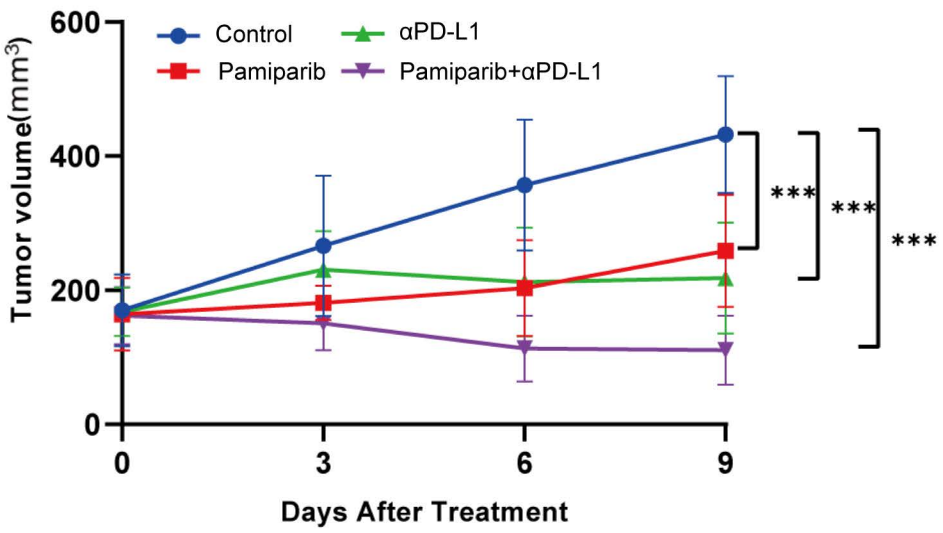
Control
αPD-L1
Pamiparib
Pamiparib+αPD-L1
Tumor volume(mm3)
600
400
200
0
0
3
6
9
Days After Treatment
***
***
***

B

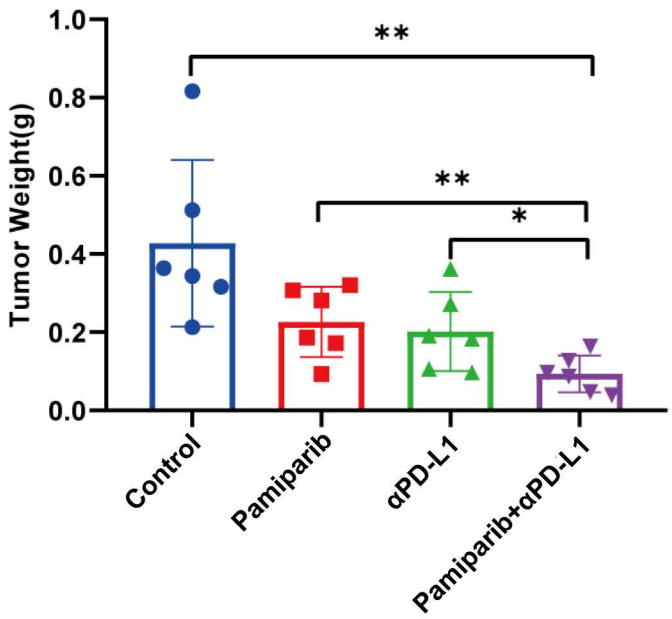
Tumor Weight(g)
1.0
0.8
0.6
0.4
0.2
0.0
**
**
*
Control
Pamiparib
αPD-L1
Pamiparib+αPD-L1

C

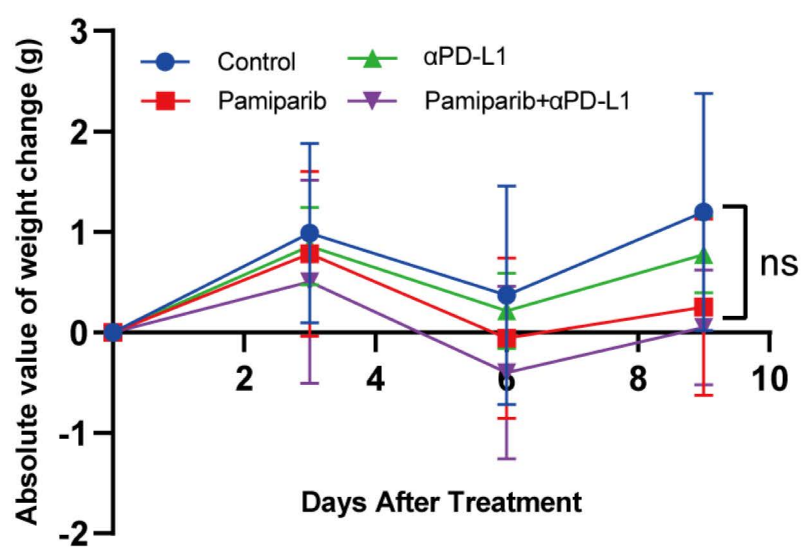
Absolute value of weight change (g)
3
2
1
0
-1
-2
2
4
6
8
10
Days After Treatment
Control
αPD-L1
Pamiparib
Pamiparib+αPD-L1
ns

D

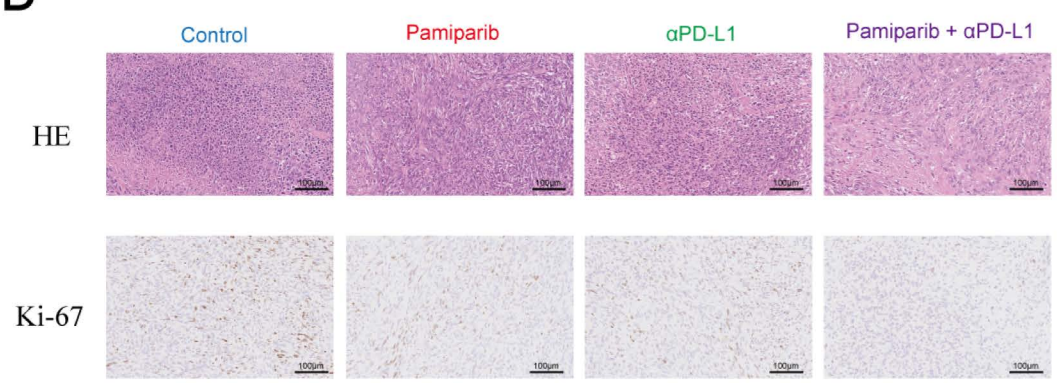
Control
Pamiparib
αPD-L1
Pamiparib + αPD-L1
HE
Ki-67

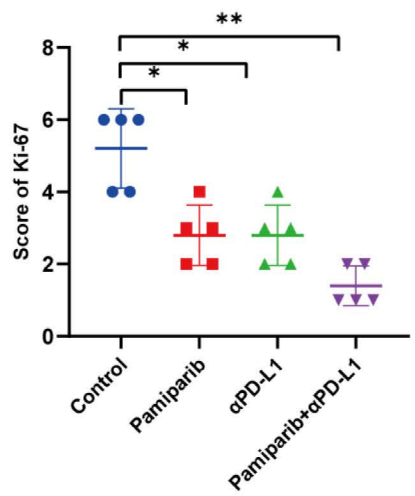
Score of Ki-67
8
6
4
2
0
**
*
*
Control
Pamiparib
αPD-L1
Pamiparib+αPD-L1

E

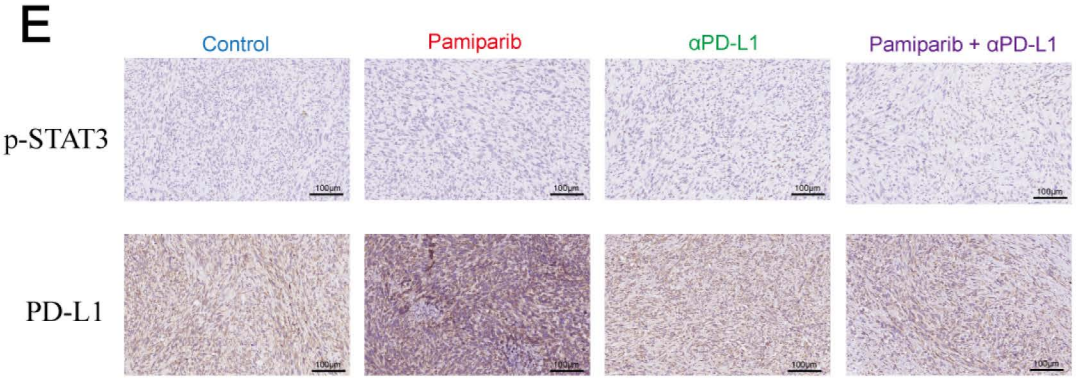
Control
Pamiparib
αPD-L1
Pamiparib + αPD-L1
p-STAT3
PD-L1

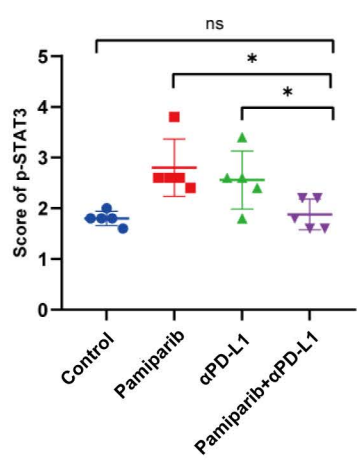
Score of p-STAT3
5
4
3
2
1
0
ns
*
*
Control
Pamiparib
αPD-L1
Pamiparib+αPD-L1

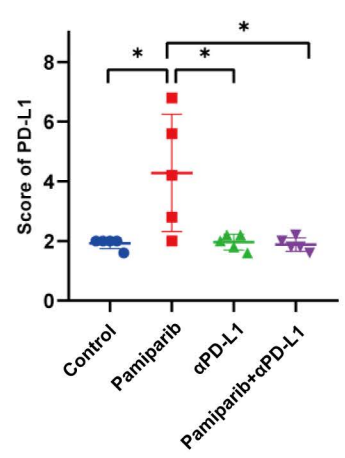
Score of PD-L1
8
6
4
2
0
*
*
*
Control
Pamiparib
αPD-L1
Pamiparib+αPD-L1

A

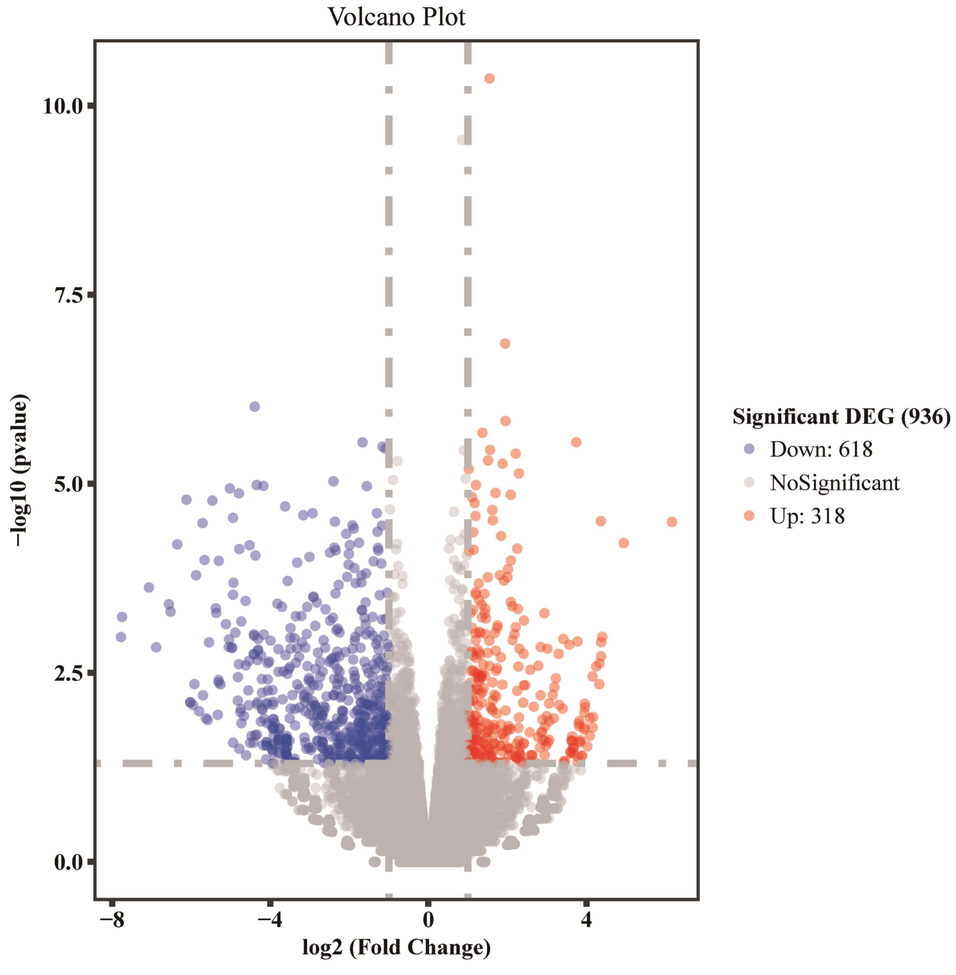
Volcano Plot
10.0
7.5
5.0
2.5
0.0
−log10 (pvalue)
−8
−4
0
4
log2 (Fold Change)
Significant DEG (936)
Down: 618
NoSignificant
Up: 318

B

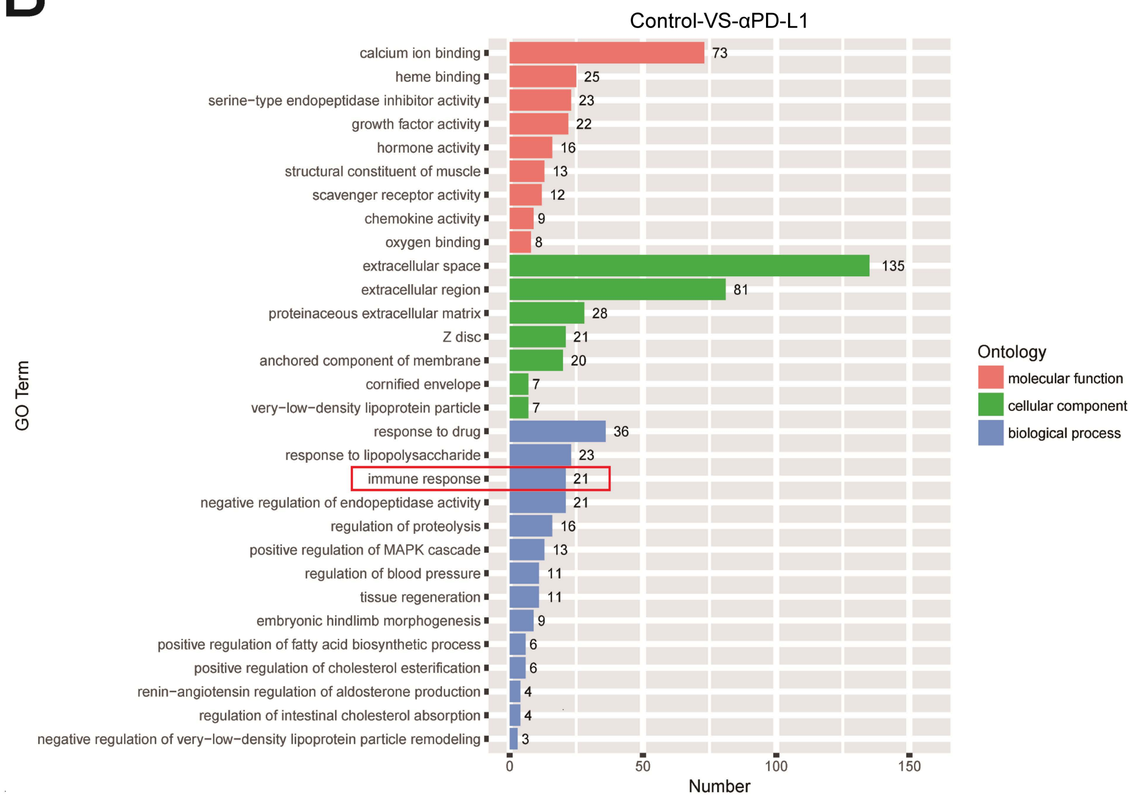
Control-VS-αPD-L1
GO Term
calcium ion binding 73
heme binding 25
serine−type endopeptidase inhibitor activity 23
growth factor activity 22
hormone activity 16
structural constituent of muscle 13
scavenger receptor activity 12
chemokine activity 9
oxygen binding 8
extracellular space 135
extracellular region 81
proteinaceous extracellular matrix 28
Z disc 21
anchored component of membrane 20
cornified envelope 7
very−low−density lipoprotein particle 7
response to drug 36
response to lipopolysaccharide 23
immune response 21
negative regulation of endopeptidase activity 21
regulation of proteolysis 16
positive regulation of MAPK cascade 13
regulation of blood pressure 11
tissue regeneration 11
embryonic hindlimb morphogenesis 9
positive regulation of fatty acid biosynthetic process 6
positive regulation of cholesterol esterification 6
renin−angiotensin regulation of aldosterone production 4
regulation of intestinal cholesterol absorption 4
negative regulation of very−low−density lipoprotein particle remodeling 3
0
50
100
150
Number
Ontology
molecular function
cellular component
biological process

C

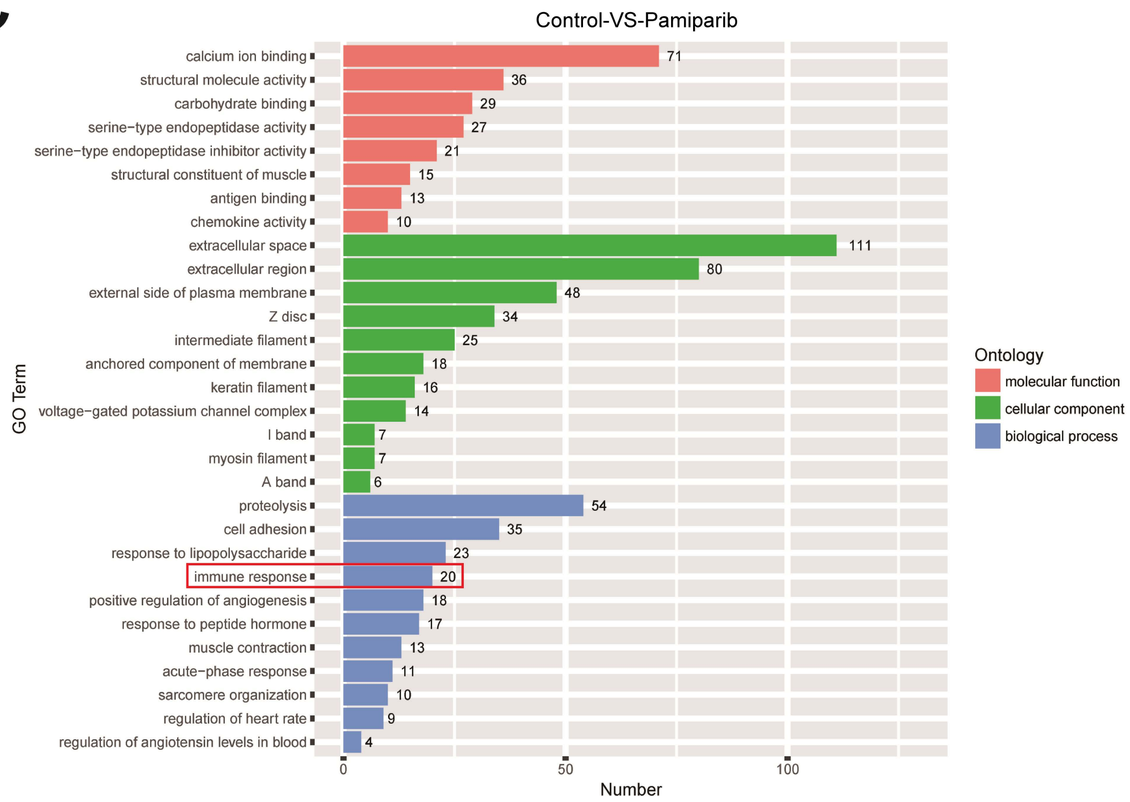
Control-VS-Pamiparib
GO Term
calcium ion binding 71
structural molecule activity 36
carbohydrate binding 29
serine−type endopeptidase activity 27
serine−type endopeptidase inhibitor activity 21
structural constituent of muscle 15
antigen binding 13
chemokine activity 10
extracellular space 111
extracellular region 80
external side of plasma membrane 48
Z disc 34
intermediate filament 25
anchored component of membrane 18
keratin filament 16
voltage−gated potassium channel complex 14
I band 7
myosin filament 7
A band 6
proteolysis 54
cell adhesion 35
response to lipopolysaccharide 23
immune response 20
positive regulation of angiogenesis 18
response to peptide hormone 17
muscle contraction 13
acute−phase response 11
sarcomere organization 10
regulation of heart rate 9
regulation of angiotensin levels in blood 4
0
50
100
Number
Ontology
molecular function
cellular component
biological process

D

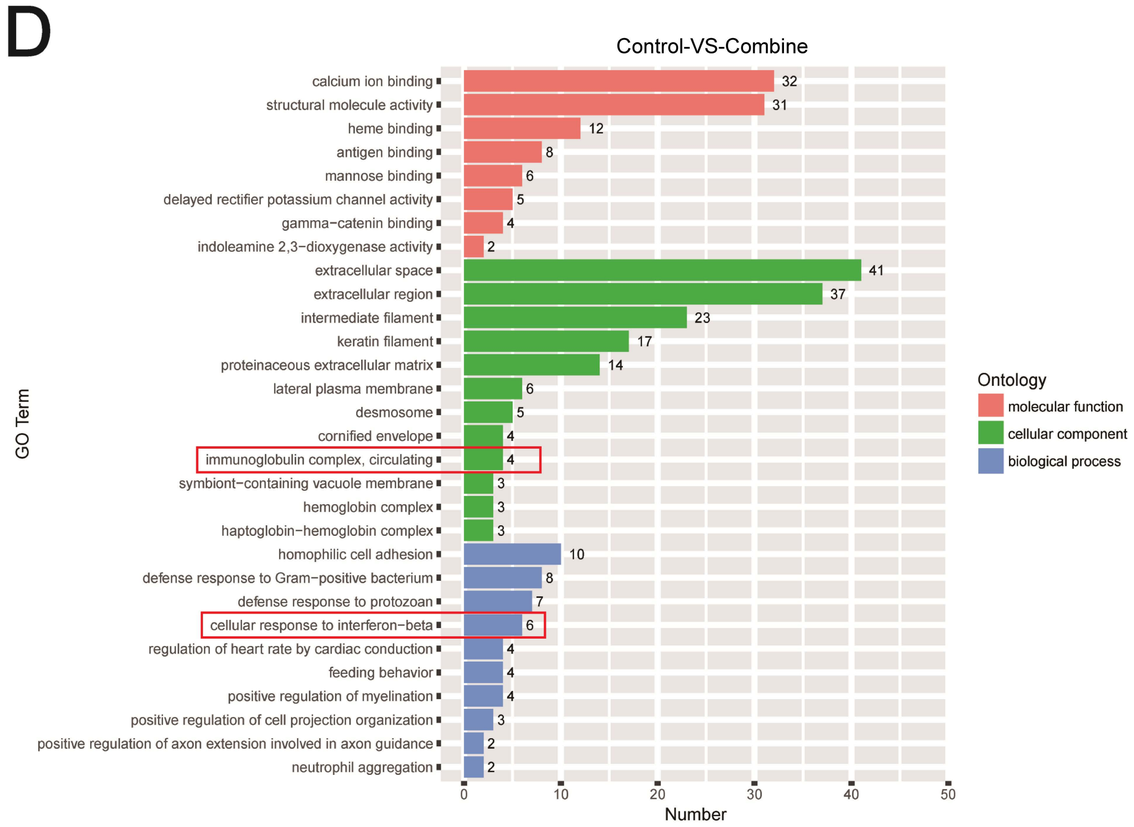
Control-VS-Combine
GO Term
calcium ion binding 32
structural molecule activity 31
heme binding 12
antigen binding 8
mannose binding 6
delayed rectifier potassium channel activity 5
gamma−catenin binding 4
indoleamine 2,3−dioxygenase activity 2
extracellular space 41
extracellular region 37
intermediate filament 23
keratin filament 17
proteinaceous extracellular matrix 14
lateral plasma membrane 6
desmosome 5
cornified envelope 4
immunoglobulin complex, circulating 4
symbiont−containing vacuole membrane 3
hemoglobin complex 3
haptoglobin−hemoglobin complex 3
homophilic cell adhesion 10
defense response to Gram−positive bacterium 8
defense response to protozoan 7
cellular response to interferon−beta 6
regulation of heart rate by cardiac conduction 4
feeding behavior 4
positive regulation of myelination 4
positive regulation of cell projection organization 3
positive regulation of axon extension involved in axon guidance 2
neutrophil aggregation 2
0
10
20
30
40
50
Number
Ontology
molecular function
cellular component
biological process

E

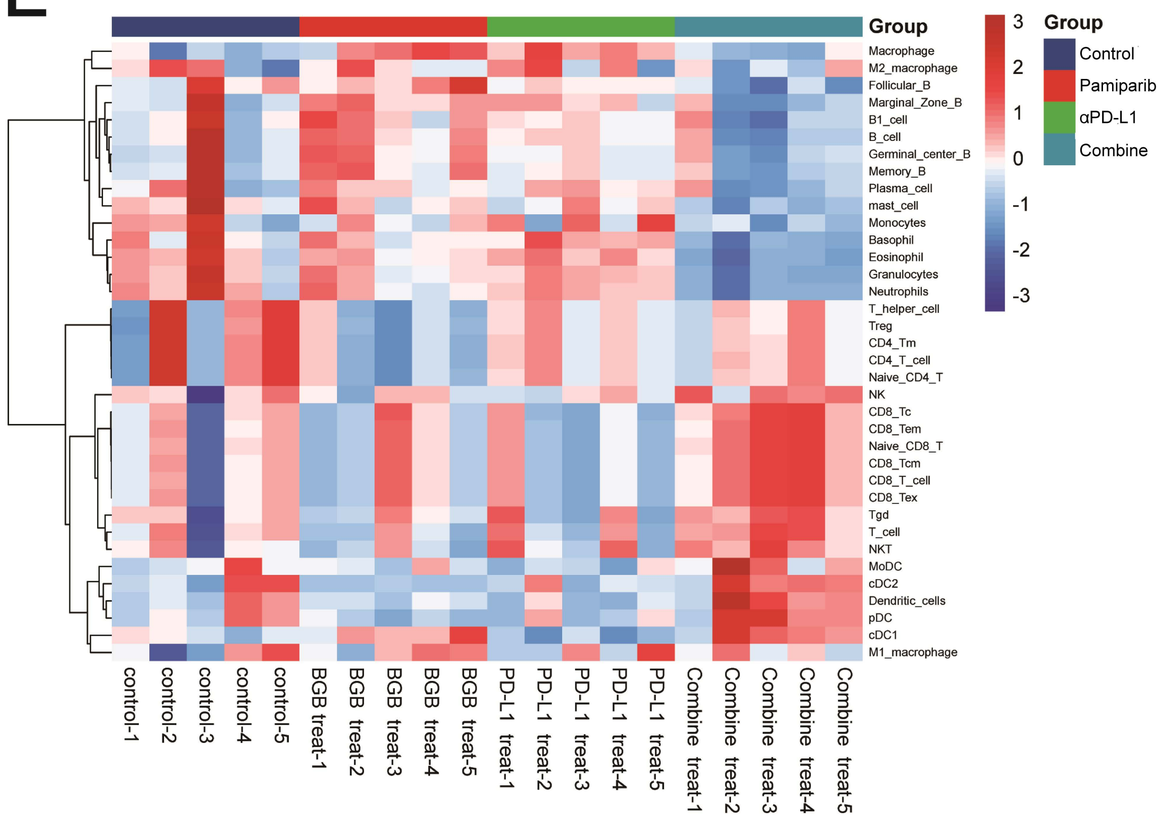
Group
Macrophage
M2_macrophage
Follicular_B
Marginal_Zone_B
B1_cell
B_cell
Germinal_center_B
Memory_B
Plasma_cell
mast_cell
Monocytes
Basophil
Eosinophil
Granulocytes
Neutrophils
T_helper_cell
Treg
CD4_Tm
CD4_T_cell
Naive_CD4_T
NK
CD8_Tc
CD8_Tem
Naive_CD8_T
CD8_Tcm
CD8_T_cell
CD8_Tex
Tgd
T_cell
NKT
MoDC
cDC2
Dendritic_cells
pDC
cDC1
M1_macrophage
3
2
1
0
-1
-2
-3
Group
Control
Pamiparib
αPD-L1
Combine
control-1
control-2
control-3
control-4
control-5
BGB treat-1
BGB treat-2
BGB treat-3
BGB treat-4
BGB treat-5
PD-L1 treat-1
PD-L1 treat-2
PD-L1 treat-3
PD-L1 treat-4
PD-L1 treat-5
Combine treat-1
Combine treat-2
Combine treat-3
Combine treat-4
Combine treat-5

F

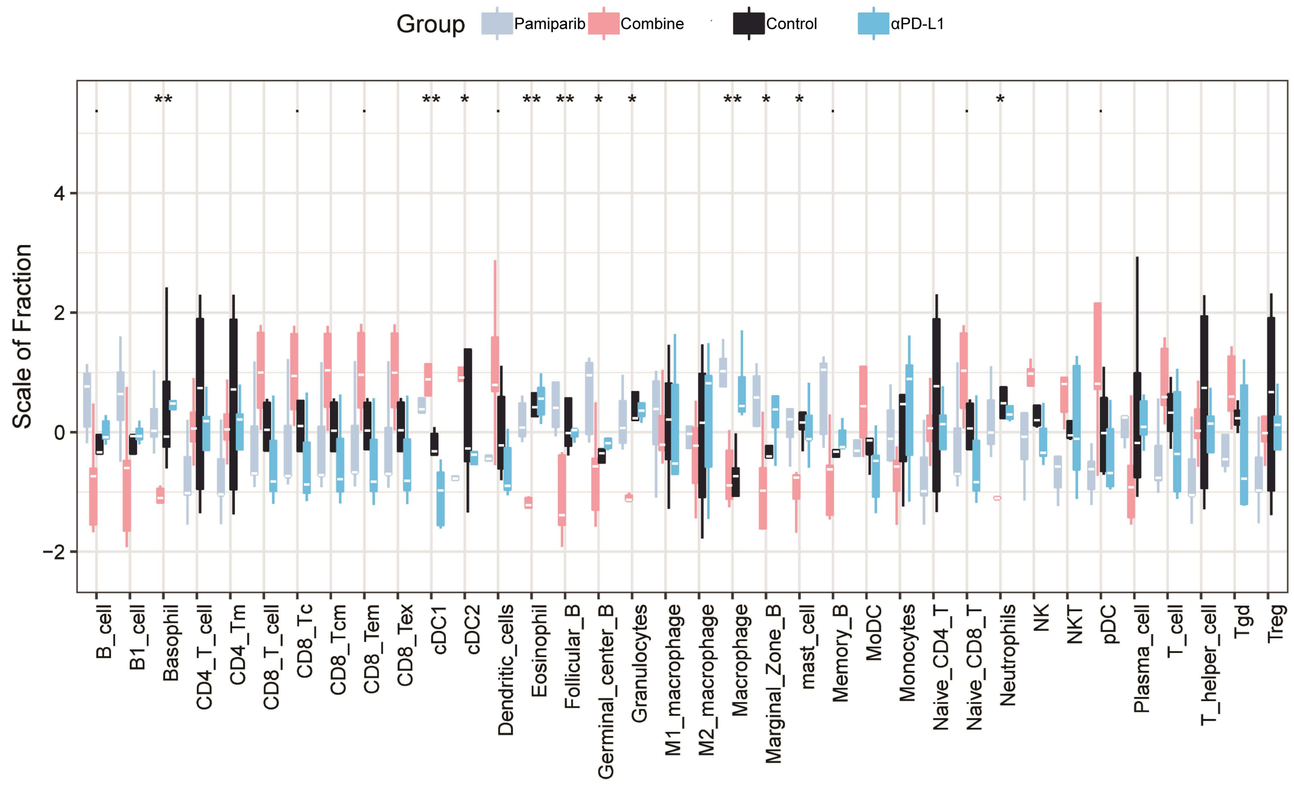
Group
Pamiparib
Combine
Control
αPD-L1
Scale of Fraction
4
2
0
−2
B_cell
B1_cell
Basophil
CD4_T_cell
CD4_Tm
CD8_T_cell
CD8_Tc
CD8_Tcm
CD8_Tem
CD8_Tex
cDC1
cDC2
Dendritic_cells
Eosinophil
Follicular_B
Germinal_center_B
Granulocytes
M1_macrophage
M2_macrophage
Macrophage
Marginal_Zone_B
mast_cell
Memory_B
MoDC
Monocytes
Naive_CD4_T
Naive_CD8_T
Neutrophils
NK
NKT
pDC
Plasma_cell
T_cell
T_helper_cell
Tgd
Treg

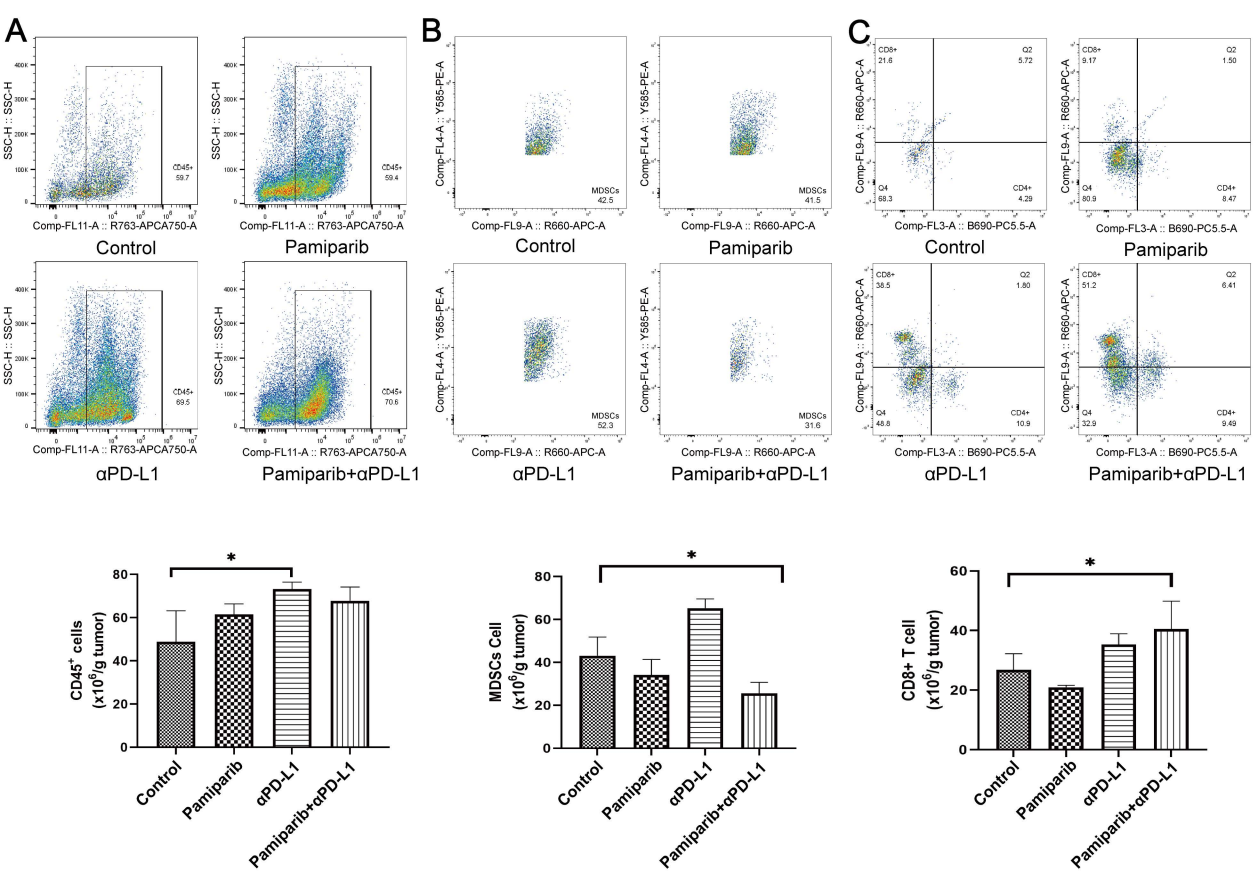
A
B
C
SSC-H :: SSC-H
Comp-FL11-A :: R763-APCA750-A
CD45+
59.7
59.4
89.5
70.6
Control
Pamiparib
αPD-L1
Pamiparib+αPD-L1
Comp-FL4-A :: Y585-PE-A
Comp-FL9-A :: R660-APC-A
MDSCs
42.5
41.5
52.3
31.6
Comp-FL3-A :: B690-PC5.5-A
CD8+
21.6
9.17
38.5
51.2
Q2
5.72
1.50
1.80
6.41
Q4
68.3
80.9
48.8
32.9
CD4+
4.29
8.47
10.9
9.49
CD45+ cells (x10^6/g tumor)
MDSCs Cell (x10^6/g tumor)
CD8+ T cell (x10^6/g tumor)
Control
Pamiparib
αPD-L1
Pamiparib+αPD-L1
*

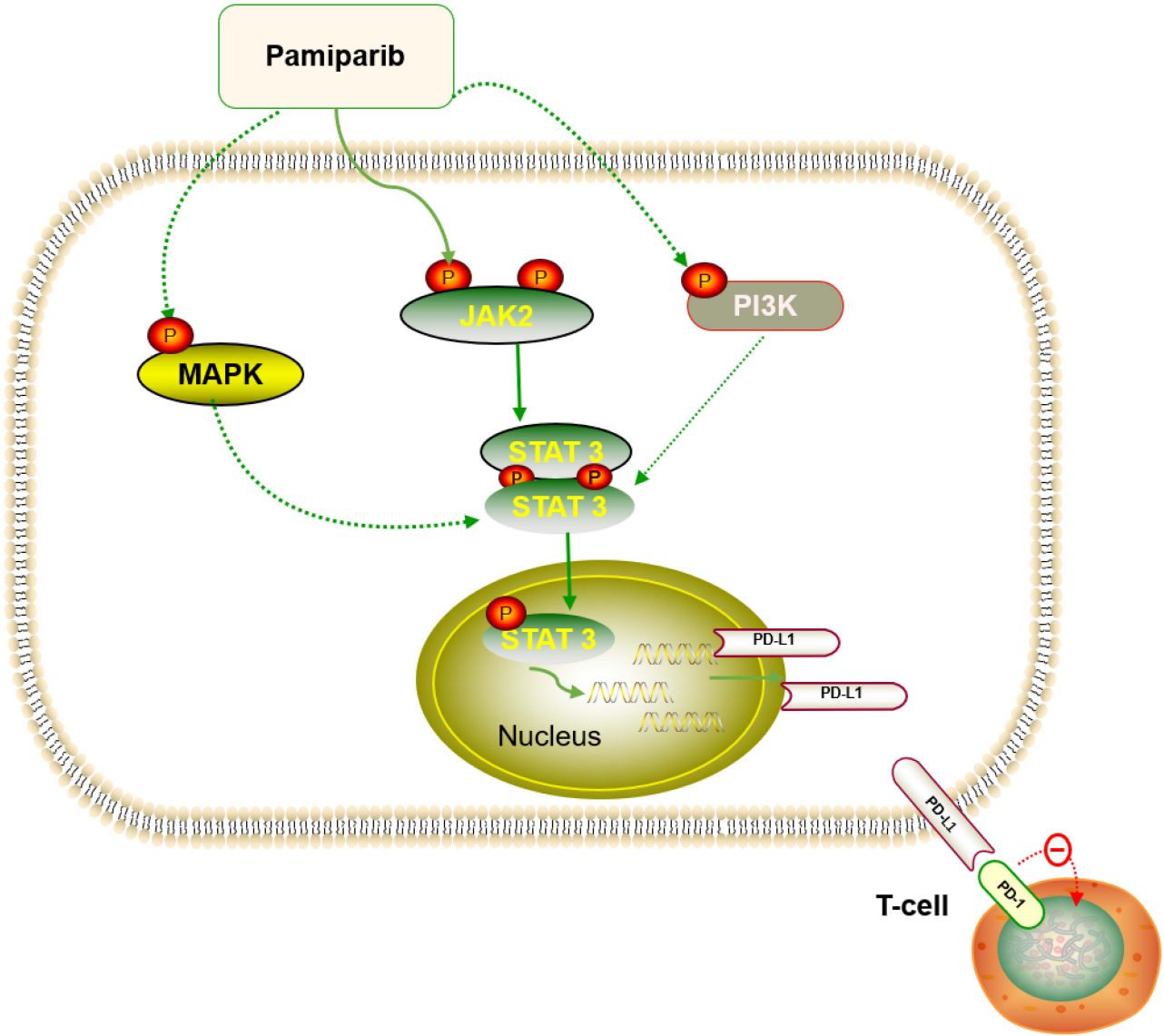
Pamiparib
P
JAK2
P
P
PI3K
P
MAPK
STAT 3
P
P
STAT 3
P
STAT 3
PD-L1
PD-L1
Nucleus
PD-L1
PD-1
T-cell

PARP Inhibitor Upregulates PD-L1 Expression and Provides a New Combination Therapy In Pancreatic Cancer

Supplementary Materials

Supplementary Figures

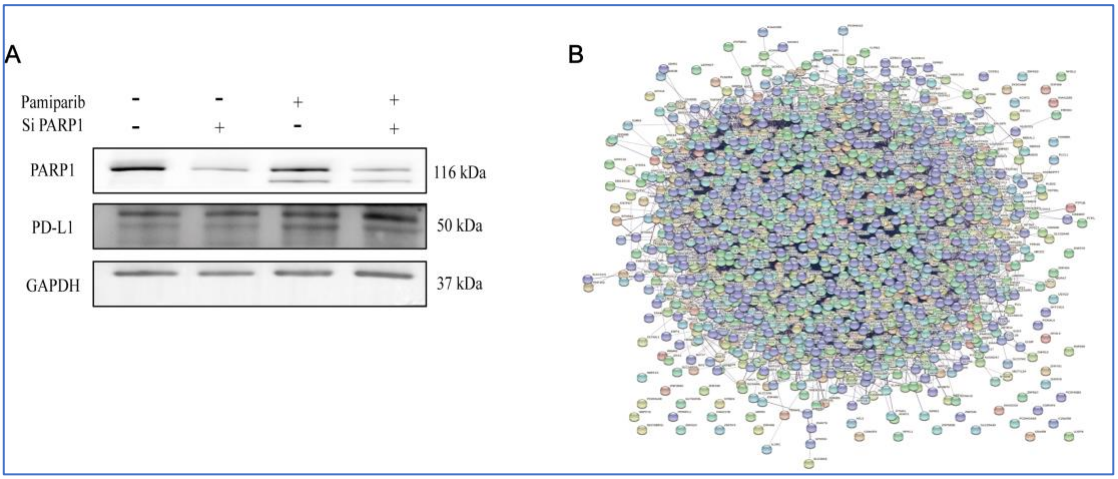

Supplementary Figure 1. Effects of PARPi treatment on PD-L1 expression. (A) PARP1 mRNA levels do not affect the upregulation of PD-L1 induced by PARPi. (B) PPI co-expression network analysis in genes associated with PD-L1 upregulation in pancreatic cancer cells.

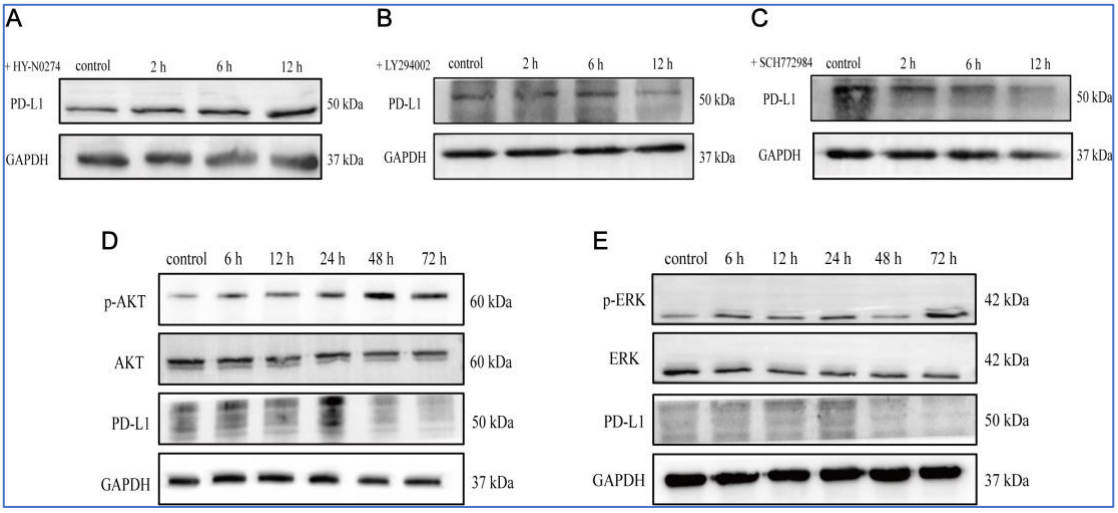

Supplementary Figure 2. PARP inhibitor treatment induces PD-L1 expression via JAK2/STAT3 pathway. (A-C) Cells were pretreated with pamiparib (100 μM) for 12 hrs and PD-L1 expression was assessed by western blotting after treatment with 20 μM of HY-N0274 (A), LY294002 (B) or SCH772984 (C), respectively, for 24 hrs. (D and E) Expression of AKT, p-AKT, ERK, and p-ERK were detected by western blotting in SW1990 cells following treatment with pamiparib (100 μM) for the indicated times. GAPDH was used as a loading control.

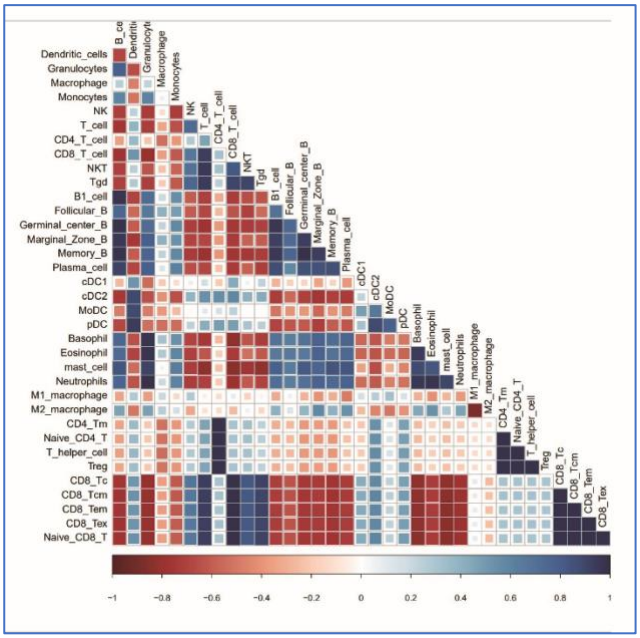

Supplementary Figure 3. Bioinformatic analysis suggests that combination therapy with PARPi and PD-L1 blocker alters the immune microenvironment.

Supplementary Tables

Supplementary Table 1. KEGG enrichment pathways of genes in PPI co-expression network.

#term ID	term description	observed gene count	background gene count	strength	false discovery rate
hsa04014	Ras signaling pathway	42	228	0.38	6.03E-05
hsa04151	PI3K-Akt signaling pathway	54	348	0.31	0.00014
hsa05200	Pathways in cancer	72	515	0.26	0.00014
hsa04659	Th17 cell differentiation	24	102	0.49	0.00017
hsa04658	Th1 and Th2 cell differentiation	20	88	0.47	0.00094
hsa04630	Jak-STAT signaling pathway	29	160	0.38	0.00094
hsa04660	T cell receptor signaling pathway	21	99	0.44	0.0013
hsa04010	MAPK signaling pathway	43	293	0.28	0.0014
hsa04012	ErbB signaling pathway	17	83	0.43	0.0043
hsa04668	TNF signaling pathway	20	108	0.38	0.0043
hsa04140	Autophagy - animal	22	125	0.36	0.0043
hsa04620	Toll-like receptor signaling pathway	19	102	0.39	0.0051
hsa05212	Pancreatic cancer	15	74	0.42	0.0074
hsa04650	Natural killer cell mediated cytotoxicity	20	124	0.32	0.0138
hsa04064	NF-kappa B signaling pathway	16	93	0.35	0.0186
hsa04662	B cell receptor signaling pathway	13	71	0.38	0.0237
hsa04210	Apoptosis	20	135	0.29	0.0252
hsa04144	Endocytosis	30	242	0.21	0.0378
hsa04066	HIF-1 signaling pathway	15	98	0.3	0.0456

Supplementary Table 2. The top 10 most significantly enriched CC, MF, BP between control and PD-L1 blocker-alone groups.

category	term	ontology	numDEInCat	numInCat	over_represented_pvalue	over_represented_FDR	GeneNumber(Up)	GeneNumber(Down)
GO:0005615	extracellular space	CC	135	1054	9.92E-41	1.34E-36	112	23
GO:0005576	extracellular region	CC	81	932	7.77E-14	5.26E-10	75	6
GO:0005578	proteinaceous extracellular matrix	CC	28	171	3.74E-09	8.44E-06	26	2
GO:0031225	anchored component of membrane	CC	20	112	2.02E-08	2.74E-05	19	1
GO:0030018	Z disc	CC	21	114	6.49E-08	7.32E-05	19	2
GO:0034361	very-low-density lipoprotein particle	CC	7	19	2.29E-06	0.001408	7	0
GO:0001533	cornified envelope	CC	7	23	5.31E-06	0.002768	6	1
GO:0042627	chylomicron	CC	5	11	1.68E-05	0.006503	5	0
GO:0034366	spherical high-density lipoprotein particle	CC	4	8	3.59E-05	0.012154	4	0

GO:0072562	blood microparticle	CC	3	3	8.57E-05	0.022236	3	0
GO:0005509	calcium ion binding	MF	73	758	5.8E-12	2.62E-08	64	9
GO:0004867	serine-type endopeptidase inhibitor activity	MF	23	146	3.43E-09	8.44E-06	22	1
GO:0008307	structural constituent of muscle	MF	13	35	5.12E-09	9.91E-06	11	2
GO:0005179	hormone activity	MF	16	107	8.91E-08	8.69E-05	13	3
GO:0020037	heme binding	MF	25	207	8.98E-08	8.69E-05	24	1
GO:0019825	oxygen binding	MF	8	23	3.07E-07	0.000277	8	0
GO:0008083	growth factor activity	MF	22	168	5.66E-07	0.000416	17	5
GO:0005044	scavenger receptor activity	MF	12	45	5.83E-07	0.000416	11	1
GO:0008009	chemokine activity	MF	9	46	9.06E-06	0.00438	6	3
GO:0070653	high-density lipoprotein particle	MF	3	3	1.03E-05	0.004502	3	0

	receptor binding							
GO:0010951	negative regulation of endopeptidase activity	BP	21	116	6.96E-10	2.36E-06	19	2
GO:0030162	regulation of proteolysis	BP	16	75	1.11E-08	1.87E-05	15	1
GO:0042246	tissue regeneration	BP	11	29	1.51E-08	2.28E-05	11	0
GO:0010873	positive regulation of cholesterol esterification	BP	6	8	6.03E-08	7.32E-05	6	0
GO:0006955	immune response	BP	21	155	3.35E-07	0.000283	14	7
GO:0032496	response to lipopolysaccharide	BP	23	174	4.86E-07	0.000387	16	7
GO:0030300	regulation of intestinal cholesterol absorption	BP	4	4	9.57E-07	0.000648	4	0
GO:0043410	positive regulation of	BP	13	62	1.65E-06	0.001065	11	2

GO:0002018	MAPK cascade renin-angiotensin regulation of aldosterone production	BP	4	4	2.85E-06	0.001676	4	0
GO:0045723	positive regulation of fatty acid biosynthetic process	BP	6	12	3.85E-06	0.002174	6	0

Supplementary Table 3. The top 10 most significantly enriched CC, MF, BP between control and pamiparib-alone groups.

category	term	ontology	numDEInCat	numInCat	over_represented_pvalue	over_represented_FDR	GeneNumber (Up)	GeneNumber (Down)
GO:0005615	extracellular space	CC	111	1054	9.54E-23	1.29E-18	30	81
GO:0030018	Z disc	CC	34	114	2.18E-18	1.48E-14	3	31
GO:0005882	intermediate filament	CC	25	77	2.53E-17	1.14E-13	1	24
GO:0009897	external side of plasma membrane	CC	48	289	3.15E-16	8.54E-13	6	42
GO:0045095	keratin filament	CC	16	38	4.58E-13	1.03E-09	1	15
GO:0005576	extracellular region	CC	80	932	2.29E-11	3.88E-08	15	65
GO:0008076	voltage-gated potassium channel complex	CC	14	54	1.22E-07	0.000103	0	14
GO:0032982	myosin filament	CC	7	13	7.74E-07	0.000524	0	7

GO:0031225	anchored component of membrane	CC	18	112	1.49E-06	0.000875	0	18
GO:0031672	A band	CC	6	11	7.2E-06	0.003165	0	6
GO:0005198	structural molecule activity	MF	36	159	1.47E-16	4.97E-13	2	34
GO:0030246	carbohydrate binding	MF	29	161	1.28E-11	2.48E-08	1	28
GO:0008307	structural constituent of muscle	MF	15	35	3.92E-11	5.89E-08	1	14
GO:0005509	calcium ion binding	MF	71	758	5.24E-10	7.1E-07	10	61
GO:0003823	antigen binding	MF	13	56	8.66E-10	1.07E-06	0	13
GO:0004252	serine-type endopeptidase activity	MF	27	207	5.39E-08	4.87E-05	4	23
GO:0004867	serine-type endopeptidase inhibitor activity	MF	21	146	3.84E-07	0.000306	12	9

GO:0008009	chemokine activity	MF	10	46	2.98E-06	0.001554	0	10
GO:0031432	titin binding	MF	6	15	1.1E-05	0.004037	0	6
GO:0008201	heparin binding	MF	23	279	2.47E-05	0.007294	1	22
GO:0006936	muscle contraction	BP	13	38	2.51E-09	2.83E-06	0	13
GO:0043434	response to peptide hormone	BP	17	82	3.5E-08	3.65E-05	8	9
GO:0006508	proteolysis	BP	54	580	5.33E-08	4.87E-05	9	45
GO:0006953	acute-phase response	BP	11	38	4.61E-07	0.000347	6	5
GO:0045766	positive regulation of angiogenesis	BP	18	105	7.01E-07	0.0005	0	18
GO:0002027	regulation of heart rate	BP	9	28	1E-06	0.000645	1	8
GO:0007155	cell adhesion	BP	35	308	1.16E-06	0.000712	4	31

GO:0045214	sarcomere organization	BP	10	31	1.66E-06	0.000937	1	9
GO:0032496	response to lipopolysaccharide	BP	23	174	1.84E-06	0.000996	3	20
GO:0006955	immune response	BP	20	155	5.05E-06	0.002533	2	18

Supplementary Table 4. The top 10 most significantly enriched CC, MF, BP between control and combination groups.

category	term	ontology	numDEInCat	numInCat	over_represented_pvalue	over_represented_FDR	GeneNumber(Up)	GeneNumber(Down)
GO:0005882	intermediate filament	CC	23	77	8.41E-22	1.03E-17	2	21
GO:0045095	keratin filament	CC	17	38	1.51E-19	6.8E-16	2	15
GO:0031838	haptoglobin-hemoglobin complex	CC	3	3	3.82E-06	0.007448	0	3
GO:0005615	extracellular space	CC	41	1054	9.62E-06	0.015914	11	30
GO:0005578	proteinaceous extracellular matrix	CC	14	171	2.44E-05	0.027392	4	10
GO:0005576	extracellular region	CC	37	932	2.47E-05	0.027392	12	25
GO:0042571	immunoglobulin complex, circulating	CC	4	16	5.66E-05	0.054739	0	4
GO:0030057	desmosome	CC	5	25	0.000167	0.138088	0	5
GO:0005833	hemoglobin complex	CC	3	9	0.000187	0.140881	0	3
GO:0020005	symbiont-containing	CC	3	6	0.000207	0.141056	3	0

GO:0005198	vacuole membrane structural molecule activity	MF	31	159	1.52E-21	1.03E-17	3	28
GO:0003823	antigen binding	MF	8	56	1.57E-06	0.004242	0	8
GO:0005537	mannose binding	MF	6	22	3.85E-06	0.007448	0	6
GO:0005509	calcium ion binding	MF	32	758	8.71E-05	0.078618	9	23
GO:0045295	gamma-catenin binding	MF	4	18	0.000413	0.254147	0	4
GO:0033754	indoleamine 2,3-dioxygenase activity	MF	2	2	0.000445	0.262191	2	0
GO:0005251	delayed rectifier potassium channel activity	MF	5	32	0.000657	0.292056	0	5
GO:0020037	heme binding	MF	12	207	0.00067	0.292056	5	7
GO:0019825	oxygen binding	MF	4	23	0.000697	0.292056	1	3

GO:0043177	organic acid binding	MF	2	3	0.00084	0.325165	0	2
GO:0042832	defense response to protozoan	BP	7	23	3.22E-07	0.00109	6	1
GO:0050830	defense response to Gram-positive bacterium	BP	8	56	1.06E-05	0.015914	5	3
GO:0035458	cellular response to interferon-beta	BP	6	27	1.69E-05	0.022955	6	0
GO:0031643	positive regulation of myelination	BP	4	9	2.63E-05	0.027392	0	4
GO:0070488	neutrophil aggregation	BP	2	2	0.000173	0.138088	0	2
GO:0031346	positive regulation of cell projection organization	BP	3	7	0.000208	0.141056	2	1
GO:0007156	homophilic cell adhesion	BP	10	126	0.000469	0.263166	2	8

GO:0048842	positive regulation of axon extension involved in axon guidance	BP	2	2	0.000503	0.263166	1	1
GO:0007631	feeding behavior	BP	4	19	0.000512	0.263166	1	3
GO:0086091	regulation of heart rate by cardiac conduction	BP	4	18	0.000525	0.263166	0	4

Supplementary Table 5. List of antibodies used for flow cytometry.

Antibody	Source	Catalog
BD Pharmingen APC-CY7 Rat Anti-Mouse CD45	BD Pharmingen	557659
BD Pharmingen PE Hamster Anti-Mouse CD3e	BD Pharmingen	553063
BD Horizon BB700 Rat Anti-Mouse CD4	BD Pharmingen	566408
BD Pharmingen APC Rat Anti-Mouse CD8a	BD Pharmingen	561093
BD Pharmingen APC Rat Anti-CD11b	BD Pharmingen	561690
BD Pharmingen PE Hamster Anti-Mouse Gr-1	BD Pharmingen	553128
BioLegend PE anti-human CD274	BioLegend	329705
BioLegend PE anti-mouse CD274	BioLegend	124307